Generation of TDGF1-knockout in a GBM cell line using CRISPR/Cas9

Master's Thesis

AALBORG UNIVERSITY

DANIEL LAMDAHL JUSTESEN

31/05/2019

Generation of a TDGF1 knockout GBM cell line using CRISPR/Cas9

Medicine with industrial specialization

9th & 10th semester - Biomedicine

AALBORG UNIVERSITY

Project period: 1st of September 2018 – 31st of May 2019

Project group: 18gr9047

Main supervisor: Meg Duroux

Co-supervisor: Johann Mar Gudbergsson, Hanne Due Rasmussen

Laboratory: Department of Immunology and Cancer Biology, (Biomedicine) Aalborg University

ECTS: 60

Author:

Daniel Justesen

_____

Daniel Lamdahl Justesen

Acknowledgements:

A special thanks to my main supervisor professor Meg Duroux, as well as my co-supervisors Johann Mar Gudbergsson and Hanne Due Rasmussen for their guidance, technical assistance and support in general throughout this master project.

I would like to thank Alexander Schmitz affiliated researcher of Aalborg University Hospital, department of clinical medicine for his help in setting up and performing Fluorescence Assisted Flow Sorting during this project. I would also like to thank Medical Laboratory Technologist Louise Hvilshøj Madsen and professor Karen Dybkær of the hematological department of Aalborg University hospital, for letting me use the Cell lab of Forskningens Hus.

A thanks to Issa Ismail Issa, fellow master student, for all your assistance in the Lab and helpful advices during the project.

Table of content

Table of contents

Abbreviations 5
1. Introduction 8
1.1 Glioblastoma multiforme 8
1.2 Treatment of glioblastoma 8
1.3 Invasiveness and Glioblastoma 8
1.4 Cripto-1 9
1.5 Cripto-1 and important signaling pathways 10
1.6 Investigating Cripto-1 in cancer using knockdown/knockout 11
1.7 various Knockout/knockdown methods 11
1.8 Aim and objective 14
2 Methods 16
2.1 Introduction 16
2.2 Design of Crispr singleguide-RNA 17
2.3 Culturing of Ntera2, U87, and HEK293T cells 17
2.4 Assessment of DNA by Gel-electrophoresis 18
2.5 Verification of PX461 plasmid 18
2.6 Oligo-duplex formation 18
2.7 Digestion of PX461 plasmid and ligation of duplexes 19
2.8 Transformation of E. coli and plasmid extraction 20
2.9 PCR on extracted plasmids 21
2.10 Assessment of cloned plasmids by sequencing 21
2.11 Generation of Cripto-1 knockout U87 cell lines 22
2.12 Extraction of genomic DNA from cell lines 23
2.13 Cripto-1 primer design and validation 24
2.14 ICE-analysis of amplicons from transfected cells 24
2.14.1 sgRNA2, sgRNA3 and sgRNA4 24
2.14.2 sgRNA1 and Non-target RNA 25
3. Results 26
3.1 Verification of CRISPR-Cas9 plasmid vector 26
3.2 Preparing PX461-vectors with sgRNA-inserts 26
3.2.1 Design of singleguide-RNA 26

3.3.1 Annealing of sgRNA-oligos 27
3.3.2 Digestion-ligation of oligos and vector 28
3.4 Design and validation of PX461-sequencing primer 29
3.5 Assessment of cloned plasmids by sequencing 30
3.6 Design and validation of the Cripto-1-primer pair 31
3.7 Optimization of transfection 32
3.8 Fluorescence assisted cell sorting of Lipofectamine transfected U87 33
3.9 Sorting of Calcium phosphate transfected U87 and Ntera2 34
3.10 ICE-analysis of amplicons from transfected cells 35
4. Discussion 38
4.1 CRISPR Cas9 vs RNAi, ZFN and TALEN 38
4.3 Stable vs. Transient expression 38
4.4 Cloning of PX461 40
4.5 Why were the ICE-Scores so low? 41
4.6 Optimizing Transfection efficiency 41
4.7 Cripto-1 and invasiveness in cancer 44
4.8 Future setup and perspectives 45
5. Conclusion 46
6. References 46
7. Appendix 53

Abbreviations

CFC - Cripto-1/FRL-1/Cryptic

CNS – Central Nervous System

CRISPR- clustered regularly interspaced short palindromic repeats

CSC – Cancer Stem Cell,

crRNA- CrisprRNA

DBs – double-strand breaks

DMEM – dulbecco's Modified Eagle Medium

E. coli- Escherichia coli

EGF- Epidermal Growth Factor,

eGFP-enhanced Green Fluorescent Protein,

EMT - Epithelial-to-mesenchymal transition

FACS - Fluorescence assisted cell sorting,

FCS- Fetal Calf Serum,

Fz - Frizzled

GBM – Glioblastoma multiforme

gDNA – genomic DNA,

GPI – glycosylphosphoatidylinositol

Indel -Insertions and deletions

KO- knockout

LB – Lysogeny Broth

LRP - low-density lipoprotein receptor-related protein

MGMT - methylguanine-DNA methyltransferase

ms – Milliseconds,

NCCs – nasopharyngeal carcinoma cells

NHEJ - Non-homologous end joining

NTC – Non-transfected control/cells

PAM – protospacer adjacent motif

PBS - Phosphate buffered saline

P/S -Penicillin and streptomycin

RISCs - RNA-induced silencing complexes, RNAi – RNA interference, RNPs – Ribonucleoproteins,

sgRNA – singleguideRNA,

shRNA- short hairpin RNA,

siRNA- short interfering RNA,

TAE - Tris-base-Acetic acid-EDTA,

TALEN- transcription activator like effector nucleases

TβR- Transmembrane serine/threonine kinase receptor

TMZ – Temozolomide

TracrRNA - Trans-activating crisprRNA,

ZFN – zinc finger nuclease

Resumé

Glioblastoma multiforme er den hyppigst forekommende og mest aggressive type kræft i centralnervesystemet. Prognosen er meget dårlig på trods af væsentlige fremskridt i radio- og kemoterapibehandling de sidste årtier. Dette skyldes blandt andet at Glioblastoma er meget invassiv, hvilket næsten umuliggør en fuldstændig operativ fjernelse. TDGF-1, der koder for proteinet Cripto-1 er et gen der regulerer stam-celle adfærd under fosterudviklingen. Genet har lav expression i det færdigudviklede væv i voksne. Undersøgelser har vist at Cripto-1 expression er øget i mange typer kræft og bidrager til patofysiologiske processer såsom EMT og vedligeholdelse af cancer stamcelle-egenskaber som medvirker til øget migration og invasiv vækst af tumor-celler. CRISPR-Cas9 gen editeringsværktøjet kan bruges til at generere Cripto-1 knockout med henblik på at studere Cripto-1's rolle i Glioblastoma. Målet med studiet er at klone singleguideRNA specifikt mod Cripto-1 ind i vektorer og transfektere disse ind i Glioblastoma cellelinjen U87. Undersøgelser vil derefter blive udført for at sikre at Cripto-1 er blevet editeret. Undervejs vil den anvendte restriktionskloningsmetode og Lipofektamin samt Calcium fosfat transfektionsmetoderne blive evalueret for at belyse om disse metoder er optimale til forberedelse af Cripto-1 editering i U87. Fire singleguideRNA som targeterer exon 3 på Cripto-1 vil blive designet vha. CrispOR og klonet ind i PX461-plasmider. Elektrokompetente *E. coli* transformeres med disse plasmider, og plasmiderne ekstraheres senere fra transformerede *E. coli* kulturer. De ekstraherede plasmider sekventeres for at evaluere om kloningen var en success. U87 transfekteres med klonede plasmider vha. Lipofektamin eller Calcium fosfat-metoden. De transfekterede celler FACS-sorteres og genomisk DNA ekstraheres. Sekventeringsresultaterne analyseres med ICE-online tool. Alignment af singleguideRNA og sekventeringsresultaterne viste at kloningen lykkes. Transfektionseffektiviteten var i gennemsnit 4.4 % med Lipofektamin, de bedste resultater kunne ikke reproduceres. Med Calcium fosfat optimering blev der opnået transfektions effektiviteter på over gennemsnitligt 10% der godt kunne reproduceres. ICE-analyse viste at U87 editeret med singleguideRNA2, 3 og 4 kun fik genereret indels i 5 % af tilfældene, og med sgRNA1 20%. Konklusionen blev at Restriktionskloning af alle singleguideRNAs blev en succes. Indels blev genereret i under 5 % af tilfældene i celler editeret med singleguideRNA2,3 og 4, mens 20% blev editeret med singleguideRNA1. Calcium fosfat havde en højere transfektionseffektivitet end Lipofektamin.

Abstract

Introduction: Glioblastoma multiforme (GBM) is the most common and aggressive form of brain cancer with a very poor prognosis despite advancements in radio- and chemotherapeutic treatments. Cripto-1 is a gene that regulates stem cell behavior during embryonic development, with low expression in the fully developed tissue of adults. Research has shown that Cripto-1 expression is increased in several cancers and contribute to pathophysiological processes that enhance migration and invasiveness. To study the contribution of Cripto-1 to GBM-pathology the CRISPR-Cas9 editing tool can be used to generate Cripto-1-knockout GBM.

Aim: To clone singleguideRNA (sgRNA) specific towards Cripto-1 into plasmids and transfect these into the GBM cell line U87 and investigate whether Cripto-1 has been successfully edited. To evaluate restriction cloning and transfection methods (lipofectamine and Calcium phosphate) and determine whether they are optimal for preparing Cripto-1 editing in U87.

Methods: Four sgRNAs targeting exon 3 on Cripto-1 was designed using CrispOr. The sgRNAs and their complementary strand was annealed into an oligo-duplex and inserted into PX461 plasmids using BbsI-restriction cleavage and ligation. Electrocompetent E. coli were transformed with digested-ligated plasmids, and plasmids were later extracted from transformed E. coli monocultures. Extracted plasmids were sequenced. U87-cells were transfected with cloned plasmids using Lipofectamine or Calcium phosphate. Genomic DNA was extracted from transfected cells isolated by Fluorescence assisted cell sorting (FACS) and sequenced. The sequencing output was analyzed using the ICE-tool.

Results: Multiple alignment between sgRNAs and sequencing output revealed that cloning of PX461 sgRNAs was successful. Lipofectamine Transfection of U87 had low efficiencies (average 4.4 %). Calcium phosphate transfection were able to generate efficiencies above 10 % after two optimizations. ICE-analysis of U87-cells edited using sgRNA2,3 and 4 showed that indels has been generated in less than 5 % of cells, while cells transfected with sgRNA1 contained indels in 20 % of the population.

Conclusion: Restriction-based cloning of all sgRNAs was a success. Indels were generated in Less than 5 % of cells edited with sgRNA2,3,4 and only 20 % edited with sgRNA1. Lipofectamine was inferior in terms of transfection efficiency, and Calcium phosphate was inferior in terms of cell viability

1. Introduction

1.1 Glioblastoma multiforme

Glioblastoma Multiforme (GBM) is a type of cancer of the Central Nervous System (CNS) (1) (2), characterized by grade 4 malignant histological features (3). It has since 2016 been grouped, by the WHO, into either an primary and secondary category depending on the presence or absence of mutations in the IDH1- and IDH2-genes. IDH-wildtype glioblastomas comprise roughly 90 % of glioblastomas and is most commonly primary glioblastomas, while the IDH- mutants are mostly secondary glioblastomas that arise from lower-grade tumors. (1) (2) The IDH-wildtype GBM occurs mostly in older people with a median age at the time of diagnosis of roughly 62 years, while the median age of diagnosis is about 44 years, among the patients afflicted with IDH-mutant GBM. (2) Every year 2-3 cases of GBM pr. 100.000 adult is observed in Europe and North America, with a slightly higher incidence in men relative to women (1). Glioblastoma multiforme is the most aggressive (3) and common form of CNS-cancer (4). The prognosis of patients afflicted with GBM is very poor with a median survival of about 12 months, after diagnosis, and only very rarely longer than two years (3)(5).

1.2 Treatment of glioblastoma

Current treatment of GBM consist of maximum safe resection, followed by radiotherapy and treatment with Temozolomide (TMZ). There is no cure for GBM, and standard treatment is mainly focused on increasing quality of life and length of survival of patients (6). Many GBM-tumors express DNA repair genes that render TMZ and radiotherapy ineffective (7). A particularly important repair molecule called methylguanine-DNA methyltransferase (MGMT) is capable of repairing bases that have been alkylated by TMZ (7). MGMT expression is impaired by MGMT promoter methylation in about 45 % of GBM-cases, making the tumor less resistant to TMZ (7). Treatment with TMZ in addition to radiotherapy increases survival with about 2,5 months in GBM patients (5). GBM is highly invasive which renders complete resection of GBM almost impossible since it would require removal of too much healthy CNS-tissue (8). For these reasons recurrence of the disease is practically inevitable after surgery (4) (6) (8).

1.3 Invasiveness and Glioblastoma

Since invasion of healthy brain tissue makes it almost impossible to completely remove GBM through surgery (8) it is important to understand its pathophysiological causes. A process known as Epithelial-to-mesenchymal transition (EMT) has been shown to be important for invasion and

migration of GBM-cells. (9) During EMT adherence proteins like E-cadherin and tight junction proteins like occludins are downregulated, while other adhesive proteins such as N-Cadherin are upregulated. The cytoskeleton is rearranged, and actin-fiber production is increased. These changes and others lead to a loss of cell contact, and a more motile and invasive phenotype, capable of migration. EMT-mediated Migration is important during embryonic development when forming the mesodermal layer that later develop into organs like bones, muscle cartilage and others. (9) Downregulation of EMT has been shown to impair the ability of GBM-cells to migrate and invade in vitro (10).

In GBM-tumors anywhere from 1% to 30 % of the tumor consist of CD133-expressing stem-like cells (11). EMT-activation has been shown to increase stem-cell-like properties in cancers including GBM (12) (13). GBM stem-like cells has been shown to be more invasive than non-stem-like GBM cells when compared in vitro and in vivo (14).

1.4 Cripto-1

Several ligands and receptors are involved in the signaling pathways promoting EMT and stem-cell maintenance (15), such as the co-receptor Cripto-1 (16) (17). Cripto-1 is encoded by the TDGF-1 gene located on chromosome 3 (18). The gene belongs to the EGF-CFC-family and is important during early embryonic development where it regulates stem cell behavior. However its expression is low in the fully developed tissue of adults (19) (20).

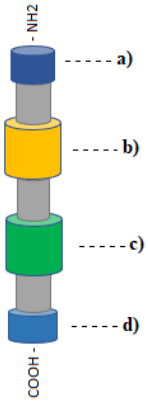

Figure 1.4: The Cripto-1 protein product. It consists of 188 amino acids, with a signaling peptide(a), an Epidermal Growth Factor (EGF)-like domain (b), a Cripto-1-FRL-1-Cryptic (CFC) domain(c), and a terminal binding site (d) for glycosylphosphatidylinositol (GPI). GPI-binding of the terminal portion, anchors Cripto-1 to the membrane where it can function as a co-receptor through its EGF-like and CFC domain, binding the Nodal-ligand the ALK4-receptor (21). The GPI-anchor can be enzymatically cleaved which will release Cripto-1 from the membrane (22)

1.5 Cripto-1 and important signaling pathways

Cripto-1 contributes to stem cell maintenance and EMT-activation through its involvement in the Wnt/β-catenin pathway (17). When wnt-ligands bind frizzled (Fz) receptors and low-density lipoprotein receptor-related protein 5 and 6 (LRP5 and LRP6), intracellular complexes that normally phosphorylate β-catenin are inactivated. This allows β-catenin to escape degradation and reach the nucleus where it can interact with transcription factors leading to expression of specific genes. Cripto-1, in its membrane-anchored form, is able to bind co-receptors of LRP5 and LRP6 (Figure 1.5a), through both its CFC and EGF domain (Figure 1.4b and c) and bind the Wnt3a-ligand, which enables enhanced Wnt/β-catenin signaling even with very low concentrations of Wnt3a. Wnt/β-catenin pathway signaling is important for maintaining stemness-properties of embryonic stem cells and cancer stem-like cells (23) (16), as well as migration and EMT-activation in some cancer cells (24) (17).

Cripto-1 is attached to the cell membrane via its COOH-terminal portion (Figure 1.4d). At the membrane Cripto-1 acts as a co-receptor for the type I activin serine-threonine kinase receptors, Alk4 and Alk7. Nodal, a ligand for these activin receptors, needs Cripto-1 to activate the Alk4 receptor. Alk4-receptor activation leads to downstream activation of intracellular signals such as Smad2 and Smad3 by phosphorylation (Figure 1.5b). Activated second messengers eventually reach the nucleus and upregulate the expression of specific genes. Nodal is capable of activating Alk7 without Cripto-1, but Cripto-1 is known to increase the sensitivity of the receptor towards Nodal. (20) The effect of Nodal activation varies, but has been demonstrated to increase migration and proliferation in some cancers, and cell growth specifically in GBM (25) (26).

Cripto-1 can directly bind the proteoglycan Glypican-1, at the membrane and induce intracellular signaling. Binding of Glypican-1 leads to activation of c-src by phosphorylation, which in turn activates the MAPK/AKT pathway (Figure 1.5c), resulting in increased cell survival, migration and proliferation (20).

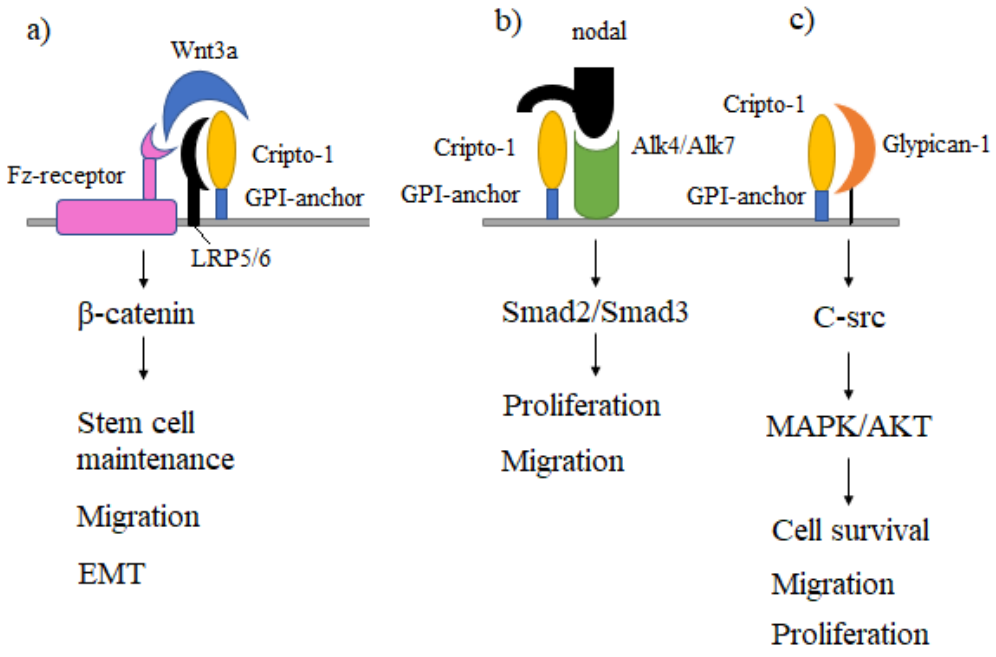

Figure 1.5: Important signaling pathways Cripto-1 is involved in. A) Cripto-1 increases the sensitivity of the Fz and LRP5/6 receptor towards Wnt3a which leads to signaling that preserves β-catenin from degradation. Intact β-catenin leads to expression of genes involved in maintenance of stem cell properties (23) (16), as well as migration and EMT-activation (17) (24) B) Cripto-1 functions as a co-receptor for the type I activin serine-threonine kinase receptors, Alk4 and Alk7 enhancing binding of the Nodal-ligand to these receptors. Receptor activation leads to phosphorylation of intracellular Smad2 and Smad3 second messengers which further downstream promote the expression of genes promoting cell differentiation and proliferation. C) Cripto-1 can bind Glypican-1 which causes phosphorylation of C-src which activates the MAPK/AKT pathway and promote proliferation, migration and survival signaling(20)(27).

In summary it is known that membrane-bound Cripto-1 is implicated in several signaling pathways that has been shown to promote Migration as well as invasiveness-related processes like EMT, and Stem cell maintenance, in some tumors (20) (16) (24) (17).

1.6 Investigating Cripto-1 in cancer using knockdown/knockout

Methods that suppress Cripto-1 expression has been useful in elucidating its role in migration and invasiveness in cancer, as well as the molecular pathways Cripto-1 is involved in. One example is a study in which siRNA-mediated Knockdown of Cripto-1 in prostate cancer cell (PCCs) revealed that high Cripto-1 expression is important for migration and invasion in vitro PCCs, and that Cripto-1 activated EMT through β-catenin (28) Another study investigated the role of Cripto-1 in nasopharyngeal carcinoma cells (NPCs) by introducing stable expression of RNA interfering Cripto-1 which resulted in reduced invasion in vitro (29).

1.7 various Knockout/knockdown methods

Knockdown of a gene of interest can be achieved using RNAi in which short interfering RNA (siRNA) or short hairpin RNA(shRNA) is introduced into cells and incorporated in the RNA-induced

Silencing complex (RISC) leading to degradation of mRNA that are complementary to the siRNA/shRNA (30).

An alternative to RNAi would be the zinc finger nuclease (ZFN) gene editing tool. ZFN, introduces double strand breaks (DBs) that is repaired by Non-homologous end joining (NHEJ). NHEJ potentially results in gene knockout. (31) DBs are introduced by the FokI nuclease, and target specificity is achieved by zinc finger proteins. Zink finger proteins each recognize and bind specific 3 bps sequences. By combining 3 to 6 chosen zink finger proteins, the ZFN-complex can be directed towards virtually any genomic target. (31)

Another option for gene-editing is the transcription activator like effector nucleases (TALEN). TALEN consists of transcription activator like effector (TALE) repeats fused to a FokI-nuclease. Each TALE repeat is specific towards a single base-pair. The FokI nuclease cleaves the DNA strand introducing DBs which leads to NHEJ. Like ZFN, TALEN thus introduces gene-knockout via NHEJ (32).

A new gene-editing tool has emerged since 2012 called: clustered regularly interspaced short palindromic repeats (CRISPR) (33). In nature CRISPR and its associated Cas-proteins provide bacteria and archaea with acquired immunity towards invading pathogens such as viruses. Once foreign DNA from an invading pathogen is recognized by the bacteria or archaea, short stretches of DNA called Spacers, are integrated into the Crispr locus of the bacteria or archaea. Recognition sites known as protospacer adjacent motif (PAM) determines the location of protospacer sequences in the foreign DNA, which are the sequences spacers will be derived from. (34) (35) Once expressed the spacers present in the Crispr loci become part of the crispr-RNA (crRNA). Since crRNA contains spacer sequences it can bind proto spacers on foreign DNA that match its spacer (Figure 1.7.1). Once bound to the matching sequence Cas-complexes, that crRNA is attached to, can facilitate cleavage of the foreign DNA, thereby conferring resistance of the microorganism towards viruses and foreign genetic material. A complementary match between protospacers and crRNA is not enough to facilitate cleavage of DNA, since the PAM-sequence needs to be present next to the protospacer sequence on the target. (36) Mutations that alter the PAM or proto-spacer sequence can thus help viruses escape recognition by crRNA (34). There are many CRISPR/Cas systems available with different PAM requirements for targeting DNA. One well known example is the Cas9-nuclease, derived from *streptococcus pyogenes*, that will only bind to and cleave DNA if a 5'NGG PAM sequence precedes the target sequence. (37)

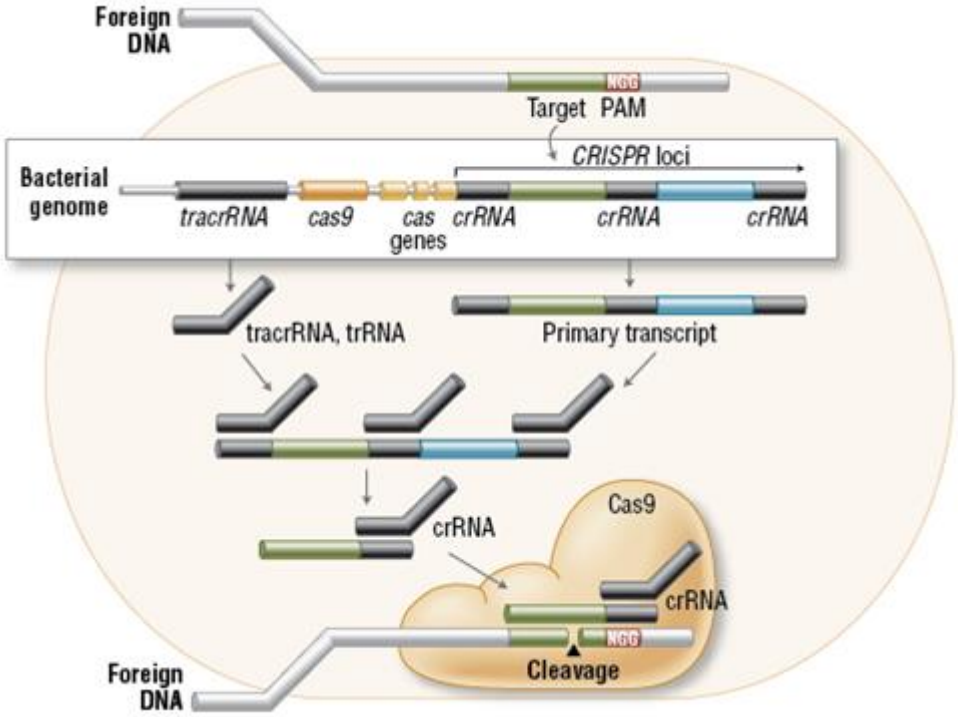

Figure 1.7.1: when invaded by viruses, certain bacteria can acquire DNA from the invading pathogen and integrate it into its Crispr-loci as a spacer. The sequences spacers are derived from are called protospacers and its location on the pathogen's genome are determined by the position of PAM-sequences, since protospacers are located adjacent to PAM. Once CrisprRNA is produced, the spacer-region is used to identify foreign DNA by complementary base pairing. The Cas9-nuclease will then cleave the DNA belonging to the invading pathogen. The Crispr-Cas9 complex will only cleave the DNA if a spacer is located adjacent to the complementary sequence. (34) (35) (36) Figure adjusted from (38).

The CRISPR loci was identified as early as 1987 in the genome of *Escherichia coli* (*E. coli)* strains by japanese scientists. By 2005 spacers in the Crispr loci were discovered to be derived from foreign genetic material and viruses (33), and by 2008 a study confirmed that the Crispr-machinery can indeed target foreign DNA directly (39). Trans-activating crisprRNA (TracrRNA), located upstream of the Cas genes and Crispr-loci was shown to have an important role in crRNA maturation in a 2011 study (40). In 2012 it was discovered that crRNA and TracrRNA can bind to each other and together form a single-RNA complex. This RNA-complex is bound by the Cas9 endonuclease and can direct it towards target DNA through its short guide sequence that is complementary to the foreign DNA. The HNH and RuvC nuclease domain on Cas9, is positioned relative to the guide-sequence in such a way that they can facilitate double-strand breaks (DBs) on target DNA once the guide-sequence has bound to the complementary sequence on the foreign DNA. (41) In 2012 a single guide RNA was engineered that retained important features from tracrRNA og crRNA such as target recognition, the ability to fuse with each other, and the ability to form a complex with Cas9. This simple system consisting of Cas9 and single guide RNA can target

any sequence positioned next to the PAM-sequence, and only requires designation of a short 20 bp guide-sequence that is specific towards the desired target. (41) (33) Once DBs has been introduced by Crispr-Cas9, cells will attempt to repair the damage by Non-homologous end joining (NHEJ). The NHEJ repair mechanism often incorrectly inserts or deletes bases when attempting to fix the breakage (Figure 1.7.2). These insertions and deletions (indel's) of bases can lead to altered reading frames which in turn can cause some bases further downstream of the DBs to be translated as a stop-codon. Crispr-Cas9 can thus disrupt expression of a gene by introducing DBs that can lead to premature stop-codons. (35)

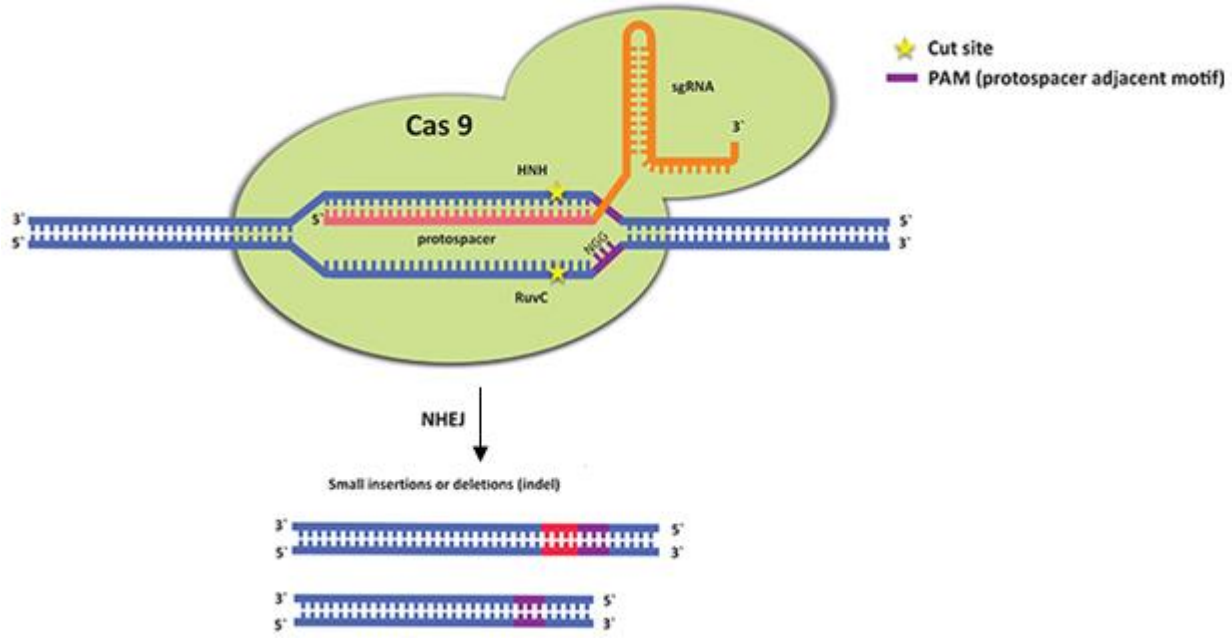

Figure 1.7.2: double strand break mediated by the Cas9-nuclease. TracrRNA and crRNA, the two RNA components of the Cas9 system, has been engineered into a singleguide RNA(sgRNA). This single RNA structure retains the ability of crRNA to bind target DNA, while the tracrRNA component binds and anchors sgRNA to Cas9. The HNH domain on Cas9 cleaves the strand that is complementary to the singleguideRNA, while the RuvC domain cleaves the opposite strand. Double-strand breaks can be repaired via the error-prone non-homologous end joining mechanism, introducing Indels (41) (35) Figure is modified from (42).

1.8 Aim and objective

The recently emerged method for introducing gene-knockout, known as CRISPR, can effectively target any sequence through its 20 bp guide-sequence if its target is positioned next to a PAM-sequence. (41) (33) Investigations has shown that Cripto-1 is involved in processes that promote tumor migration and invasiveness in various cancers. knockout/knockdown methods has played an important role in these investigations. (28) (29) Since invasiveness of GBM enables it to avoid

complete removal via surgery (8), Cripto-1 in would be an interesting gene to edit using the CRISPR-Cas9 technique.

Aim:

- To design and clone singleguideRNA's (sgRNAs) targeting Cripto-1 into plasmids containing sequences necessary for gene-editing.
- To transfect U87 with cloned plasmids and assess whether Cripto-1 has been successfully edited.
- To evaluate the restriction cloning and transfection methods (lipofectamine and Calcium phosphate) employed in this study and determine whether they are optimal for preparing Cripto-1 editing in a GBM cell line, like U87.

2 Methods

2.1 Introduction

In this section the steps utilized to introduce knockout of Cripto-1 in U87 will briefly be covered. The PX461 vector will first be introduced since several methods employed are dependent upon the features of the vector (such as flowsorting of cells thanks to the eGFP-gene).

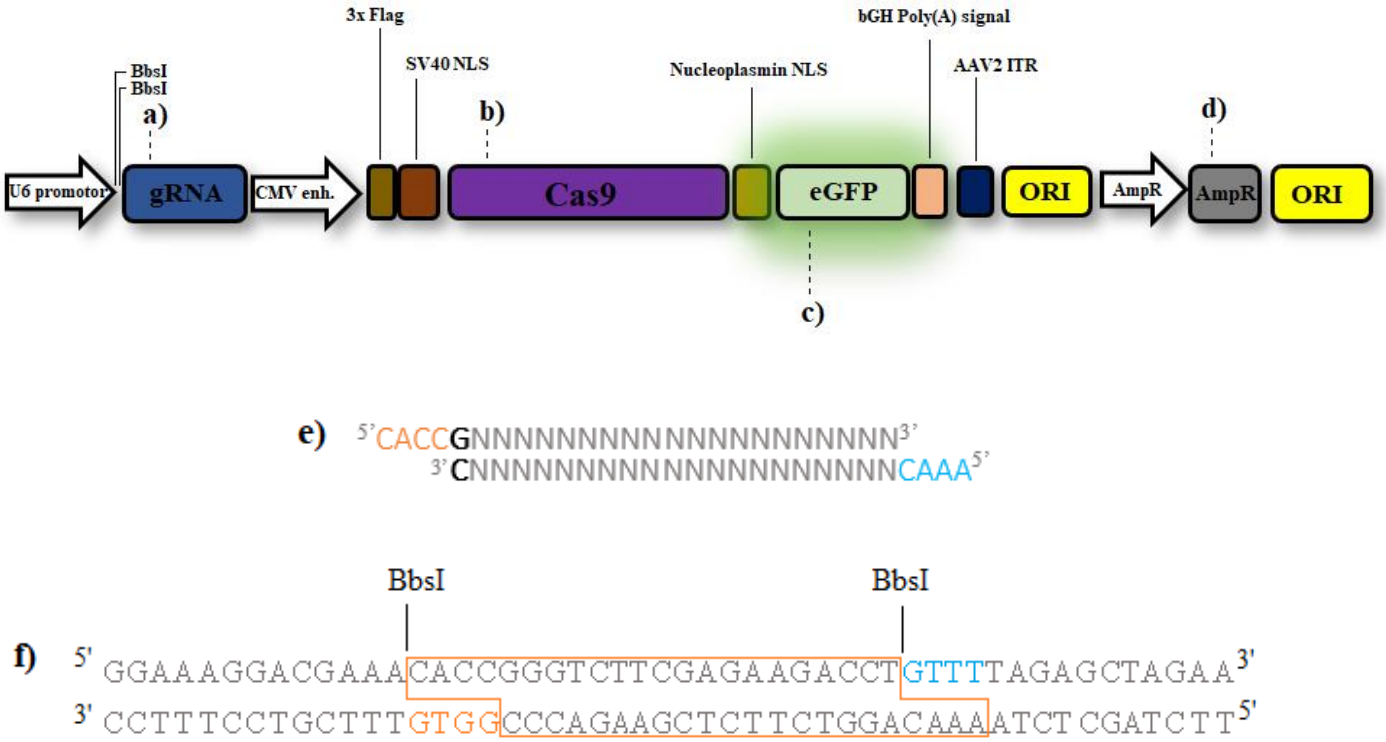

Figure2.1: Content of the PX461 plasmid. With origin of replication (ORI) sites shown as yellow boxes, and promotors displayed as white arrows. a) the guide-RNA-scaffold sequence encodes the RNA structure that forms a complex with the Cas9 nuclease. The guide-RNA scaffold is preceded by a BbsI-cutsite region. b) the Cas9-sequence encodes the Cas9-nuclease that cleaves the DNA-strand. c) the eGFP-sequence encoding the enhanced Green Fluorescent Protein (eGFP). eGFP emits green light when exposed to light in the blue to ultra violet range, a feature used in this study to identify and isolate transfected cells. d) The ampicillin resistance gene was used to isolate E. coli strains transformed with the vector, by streaking them on ampicillin containing agar. e-f) a closer look at the BbsI-cutsite area of PX461, and an example of a guide-duplex ready for integration into PX461. f) BbsI-restriction cleavage removes the 22 basepairs (within the red box). BbsI cuts asymmetrically thus creating overhangs, ($^{5'}GGTG^{3'}$ and $^{5'}GTTT^{3'}$) that are no longer basepaired. e) four bases called linker-oligos, that are complementary to the overhangs generated on PX461, must be present at the 5'end of each strand, to enable integration of singleguide-duplexes during the cloning procedure. Notice the guanine base and its complementary cytosine highlighted in bold on each strand. The guanine is added to enhance expression of the singleguideRNA since U6 promotor transcription is initiated more effectively if guanine is the first base at the transcription start site (43).

To generate cripto-1 knockout cell lines the pSpCas9n(BB)-2A-GFP (PX461)-vector (addgene: #48140) will be utilized (See Figure2.1). The vector contains the gRNA-scaffold (Figure 2.1a) and Cas9-nuclease sequences (Figure 2.1b) necessary for production of the Crispr-cas9 complexes. As described in the introduction section 1.7 the Cas9-endonuclease needs a 20 bp sgRNA sequence to direct it towards its genomic target. SgRNA (Figure 2.1e) specific towards the Cripto-1 gene will therefore be designed and subsequently inserted at the BbsI-cleavage site. BbsI-restriction cleavage of PX461 will remove 22 bp's (Figure 2.1f) and enable insertion of the chosen guide-sequences using a Ligase-enzyme. Once PX461-vectors has undergone this treatment they can be inserted into E. coli strains by electroporation. With subsequent growth of bacteria on agar containing ampicillin we expect only bacteria transformed with the PX461-vector to survive, since they possess the ampicillin resistance gene (Figure 2.1d). Bacterial colonies containing the vector can then be cultured until they reach concentrations high enough for plasmid extraction. Once extracted the insertion of the singleguide sequence can be verified by sequencing. If positive, our cells of interest can be transfected with the verified plasmids. Since the PX461 vector contains the eGFP-gene (Figure 2.1c), transfected cells can be isolated from non-transfected by fluorescence assisted cell sorting (FACS) which can sort cells based on fluorescence detected. After isolation the transfected cells will be cultured until we have enough cells for extraction of genomic DNA (gDNA) which will then be used to analyze efficiency of Cripto-1 editing.

2.2 Design of Crispr singleguide-RNA

The Crispr design tool CrispOr (44) (45).was used for singleguide-RNA design. The *Cripto-1* exon 2 and exon 3 sequence was each inserted in the CrispOr input sequence box to find possible guides with target-sites on these exons. To identify possible off-targets the Genome database was set to:*" Homo sapiens – human – UCSC Dec. 2013 (GRCh38/hg38) + SNPs: dbSNP148, kaviar".* The protospacer Adjacent Motif (PAM) was set to*;"20bp-NGG – Sp Cas9, SpCas9-HF1, eSpCas9 1.1"*, before submitting the search.

2.3 Culturing of Ntera2, U87, and HEK293T cells

HEK293T, Ntera2 and U87 cell lines where cultured in either T175 or T75 flasks containing Dulbecco's Modified Eagle Medium (DMEM, Gibco, Catalog # 31966-021 and Catalog# 21969-035) supplied with 10 % Fetal Calf Serum (FCS, Gibco, Catalog # 10270-106) and 1 % penicillin

and streptomycin (P/S). Cells were grown in a humidified incubator at 37 °C and 5% CO_2. Upon reaching 80-90 % confluency cells were washed, trypsinized and passaged into new flasks.

2.4 Assessment of DNA by Gel-electrophoresis

To visualize DNA in solutions (PCR-products, cloned plasmids etc.) gel electrophoresis was performed. The percentage of agarose in gels used was dependent upon expected DNA-fragment size. 1-2% Agarose was dissolved in 1X TAE-buffer (Tris-base 40 mM, Acetic acid 20 mM, EDTA 1 mM) and heated in a microwave until no agarose-fragments could be observed. Gelred (Biotum, Catalog #41003) was diluted 10.000-fold into the agarose-solution before it solidified. 6X loading dye (Thermo scientific, Catalog #R0611) was added to the DNA-containing solutions that were loaded onto the gel. A Generuler 100bp plus (Catalog #SM0321) or Generuler 1 kb (Catalog #SM0313) Ladder were run on gels next to samples dependent upon expected DNA-fragment size. The gel was run at either 50 or 100 Volt for 20-35 minutes. Gels were examined with an Odyssey Fc imaging system (Licor Biosciences) using the 600 nm channel.

2.5 Verification of PX461 plasmid

To verify the PX461-plasmid from add-gene, PX461 was digested with XbaI (Fermentas, Catalog #FD0684) and NotI-endonuclease (Fermentas, Catalog # ER0591) alone, as well as a double digest with both XbaI and NotI (see Table 2.5). Digestion was performed at 37 °C for two hours. These three digests were run on a 1 % agarose gel next to an undigested PX461 control and a 1 Kb Ladder.

Digestion mixture	Volume
Enzyme (XbaI or/and NotI)	0,5 µl (pr. enzyme)
NEBuffer 3.1 (10X)	5 µl (1X)
DNA (PX461 stock conc. 313 ng/µl)	3,2 µl (1 µg)
ddH_2O	Up to 50 µl

Table2.5: 1 µg of DNA was mixed with 1X NEBuffer 3.1 (New England Biolabs, Catalog # B7203S) and enzymes as well as ddH_2O up to a volume of 50 µl.

2.6 Oligo-duplex formation

Before the sgRNAs mentioned in the section 2.2 could be introduced into the PX461 vector, it first needed to be annealed with a complementary strand, to form duplexes.

1 µl of each complementary single-stranded oligo, listed in Table 2.6, were mixed with 1 µl T4 DNA-ligase buffer (Thermo Scientific, Cat. No. #B69) and diluted 10-fold in nuclease-free water to a concentration of 10 pmol/µl. The mixed oligos were heated to 95 °C for 5 min. and subsequently cooled to 25 °C for 45 min. using a T100 Thermal cycler (Bio-Rad, catalog # 1861096). The annealing product were diluted 250-fold. Ten µl of oligo-dilution were run on a 2% agarose gel using single stranded oligos as control, to assess whether oligos had successfully been annealed.

	Oligo1	Oligo2
sgRNA1	*5' CACCGTCCCAGCGTGTGCCGCCCAT 3'*	*5'AAACATGGGCGGCACACGCTGGGAC 3'*
sgRNA2	*5' CACCGTCGTCCATCTCGGGGATACC 3'*	*5'AAACGGTATCCCCGAGATGGACGAC 3'*
sgRNA3	*5' CACCGCCCAGCGTGTGCCGCCCATG 3'*	*5' AAACCATGGGCGGCACACGCTGGGC 3'*
sgRNA4	*5' CACCGTCCCCATGGGCGGCACACGC 3'*	*5' AAACGCGTGTGCCGCCCATGGGGAC 3'*
Non-targetRNA	*5' CACCACGGAGGCTAAGCGTGTTT 3'*	*5' AAACACGCTTAGCCTCCGTGGTG 3'*

Table 2.6: Two oligos for each chosen sgRNA. Oligo1 contains the actual sgRNA sequence and oligo2 a complementary sequence to the sgRNA. The oligos contain the relevant overhangs as well as the added guanine, and its complementary cytosine mentioned in figure 2.1.

2.7 Digestion of PX461 plasmid and ligation of duplexes

After oligo-duplex formation, the annealing-product are introduced into PX461-plasmids at the BbsI restriction cut-sites.

Digestion ligation mixture		Thermal steps
X µl	PX461 plasmid (100 ng)	
2 µl	Annealed oligo-duplexes (0,04 pmol/µl)	6 cycles, each consisting of:
2 µl	10X Tango buffer	23 °C for 5 minutes
1 µl	DDT (10 mM)	37 °C for 5 minutes
1 µl	dATP (100 mM)	
1,5 µl	BbsI (10.000 U/ml)	Total time: 60 minutes
1 µl	T7 DNA ligase (3.000.000 U/ml)	
Y µl	ddH20 up to 20 µl	
Final volume: 20 µl		

Table 2.7: 100 ng PX461 plasmid were mixed with 2 µl annealed oligo-duplex for a final concentration of 0,004 pmol/µl. 1 µl DDT and dATP(Thermo Scientific,Catalog# R0141) were added to a final concentration of 0,5 mM. Tango buffer (Thermo Scientific, Catalog# BY5) was diluted ten-fold in the mixture. 1 µl (3.000 Units of) of T7 DNA Ligase (New England Biolabs, Catalog# M0318L) was added. 1,5 µl (15.000 units) BbsI (New England Biolabs, Catalog# R0539S) was added.

The digestion-ligation reaction of the mixture mentioned in Table 2.7 was performed using a T100 Thermal cycler (Bio-Rad, catalog # 1861096) running 6 cycles each consisting of 5 min. at 23 °C for ligation and 5 min. at 37 °C for digestion. The ligation product was compared to a PX461-vector control on a 1% agarose gel.

2.8 Transformation of E. coli and plasmid extraction

Two µl of digestion-ligation product, was mixed with 40 µl suspension containing electrocompetent E. coli from the NEB 10-beta kit (New England Biolabs, Catalog # C3020K), and transferred to 0,2 cm gap cuvettes. DNA from the ligation product were introduced into the bacterial strain by electroporation at a voltage of 2,5 kV and a time constant of about 5 milliseconds (ms), using a Micropulser (Bio-Rad, Catalog # 165-2100). The electroporated bacteria were resuspended first in 100 µl NEB 10-beta/Stable Outgrowth Medium (New England Biolabs, Catalog # B9035S) which were immediately added to 1 ml Lysogeny Broth (LB) medium and allowed to recover for 1 hour at 37 °C while shaking at 155 rpm. Thirty µl of the suspension was streaked on Ampicillin-containing LB-agar and plates as well as agar-plates without ampicillin and incubated overnight at 37 °C. An electroporated suspension not mixed with annealed oligos was also plated on ampicillin-containing LB-plates as a negative control. E. coli mixed with the pUC19 Vector from the NEB 10-beta kit, electroporated and streaked on LB-agar with ampicillin was also included as a positive control. The following day fresh colonies were picked, from the ampicillin-containing LB-plates and transferred to tubes containing 5 ml selection medium (LB-medium containing ampicillin) and incubated at 37 °C overnight.

The next day plasmids were extracted from the bacteria-in-suspension using the GeneJET plasmid miniprep kit (Thermo Scientific, Catalog # K0502). Briefly the Bacteria-in-supension was centrifuged for 5 min. at 12.000 G and 20 °C and pellet resuspended in Resuspension solution containing RNase A and transferred to a 1.5 ml tube. Lysis solution was added as well as Neutralization solution after 4 min. and the solution was centrifuged (1 min. at 12.000 G and 20 °C). The supernatant was incubated on the silica membrane of a GeneJET spin column for 3 min. to bind plasmids to the column before centrifugation for 1 min. The columns were washed twice by adding Wash buffer and centrifuged for 1 min. The spin column was transferred to a 1.5 ml tube and plasmids were eluted by adding elution buffer (incubated on membrane for 2 min.) and subsequent centrifugation for 2 min. All centrifugation steps were carried out at room temperature and 12.000 G.

DNA-concentrations and purity ratios of solutions containing the extracted plasmids, were assessed using a DS-11 FX spectrophotometer/Fluorometer (DeNovix). Solutions with a 260/280 nm absorbance ratio close to 1.8 (above 1.6 and below 2.0) as well as a 260/230 nm ratio between 2.0 and 2.2, were considered pure.

2.9 PCR on extracted plasmids

To assess whether cloning of PX461 succeeded the PX461-primer pair (See Table 2.10) was designed using the Eurofins Sequencing Primer Design Tool (Eurofins Genomics, Tubeseq). The primer pair amplifies a 527 bp region from PX461 containing the BbsI cut-site. The PX461 primers was used once to amplify PCR-products that were later sequenced and later used as a sequencing primer (the PX461 Forward) premixed with extracted plasmids sent for sequencing. The PCR-product sent for sequencing was generated mixing the primer pair with plasmids extracted from transformed bacteria (see section 2.8) as template. Primer and template were mixed with Dreamtaq PCR Mastermix (Thermo scientific, Cat. No.: K1081) and diluted in ddH_2O (Table 2.9). Amplicons were run on a 1.5 % agarose gel, next to an amplicon of PX461 as control.

PCR-mixture concentrations	Working	Thermal cycler settings		
PX461 vector	x µl (1 ng)	1 cycle	– 95 °C	(2 min.)
2X Dreamtaq PCR Mastermix	12,5 µl (1X)	35 cycles	– 95 °C	(30 sec.)
PX461 Forward	x µl (0,2 µM)		56 °C	(30 sec.)
PX461 Reverse	x µl (0,2 µM)		72 °C	(1 min.)
ddH_2O	up to 25 µl	1 cycle	– 72 °C	(10 min.)

Table 2.9: PCR was performed at an initial cycle of denaturation (95°C), 35 cycles of denaturation (95°C) annealing (56°C) and extension (72°C), and a final cycle of extension (72°C).

2.10 Assessment of cloned plasmids by sequencing

To assess whether plasmids isolated from colonies contained the sgRNA sequences, 15 µl of extracted plasmid-solution were transferred to 1,5 ml tubes and mixed with 2 µl of the forward PX-461 primer shown in Table 2.10.

Primer name	Sequence	Length
PX-461 Fw	*5'GAGGGCCTATTTCCCATGATTCC'3*	*23 bp*
PX-461 Rv	*5'AGTCCCTATTGGCGTTACTATTG'3*	*23 bp*
Cripto-1 Fw	*5'CTGTGGTCTTGTCCTTGTGATGA'3*	*23 bp*
Cripto-1 Rv	*5'CCGCCCCTCTGAATTGCTTACT'3*	*22 bp*

Table 2.10: Primers used in this study. Both PX461 primers anneal within 300 bp's distance from the BbsI-cutsite on the PX461 plasmid. The amplicon generated by the Cripto-1 primer pair are 877 bp in length and includes exon 3 on the *Cripto-1* gene.

The samples were sent to Eurofins genomics labs for sequencing. The identified bases derived from the sanger output, were aligned with sgRNA mentioned in Table 2.6, to assess whether the guides had been introduced into the plasmids. Alignment was performed using CLC sequence viewer 8.0.0.

2.11 Generation of Cripto-1 knockout U87 cell lines

Once successful cloning of PX461 was confirmed by sequencing, transfection of U87 cells with cloned plasmids was performed to generate Cripto-1 knockout cells.

Transfection of U87 with uncloned PX461 using Calcium phosphate and Lipofectamine was optimized several times to arrive at the concentrations of reagents and DNA, mentioned in table 2.11.1 and 2.11.2. Transfected cells were assessed for eGFP-percentage in the FITC-A channel using a CytoFLEX S cytometer (Beckmann Coulter). Cell viability was assessed by adding one drop of Propidium Iodide (Invitrogen, Catalog #R37169) to samples and measuring signal in the PE-A channel. Cells were gated in FSC-A/SSC-A-plot. A vertical border was set in the FITC-A channel using non-transfected controls (NTC) to identify eGFP-signaling. Samples with no addition of Propidium Iodide was used to set a vertical border in the PE-A channel for discrimination of live and dead cells.

The first transfection with cloned plasmids was performed using the lipofectamine method and only with sgRNA2, sgRNA3 and sgRNA4, since cloning of Non-target RNA and sgRNA1 hadn't succeeded yet.

Lipofectamine mixture pr. 24-well	
Lipo-mix -	2 µl L3000 reagent
	23 µl DMEM
DNA-mix -	2 µl P3000 reagent
	x µl (1 µg) DNA (sgRNA2,3 or 4)
	x µl DMEM
Total volume – 50 µl (once mixed)	

Table 2.11.1: Lipofectamine-mixture used for each well. The lipo- and DNA-mix was prepared separately, mixed and then incubated for 10-15 min. in the dark at room temperature before being applied to the wells.

The L3000 and P3000 reagent from the Lipofectamine 3000 kit (Thermo scientific, Catalog# L3000015) were used for transfection of U87 with sgRNA2, 3 and 4-containing plasmids. Wells of 24-well plates were coated with the mixture shown in Table 2.11.1. Five hundred µl culturing-medium was added to the coated wells followed by addition of 0,2 * 10^6 U87 cells pr. well.

The second transfection of cloned plasmids was performed using the Calcium phosphate method. U87 was transfected with sgRNA1 and Non-target RNA-cloned plasmids. Cells were plated in 100-mm dishes and transfected when covering approximately 50 % of the surface.

Calcium phosphate mixture pr. 100-mm dish	
Solution A -	36 µl (2M) $CaCl_2$
	x µl (20 µg) DNA (sgRNA1 or Non-target RNA)
	x µl up to 300 µl tissue Culture Sterile Water
Solution B -	300 µl 2X Hepes Buffered Saline (HBS)
Total volume	- 600 µl (once mixed

Table 2.11.2: Mixture applied to each dish. Solution A was added to B under aeration.

The mixture in Table 2.11.1 was prepared using components of the Calcium Phosphate Transfection Kit (Invitrogen, Catalog # K2780-01). The mixture was incubated for 30 min. and applied to dishes dropwise. Pictures were taken of the dishes 24 and 48-hours post-transfection using a Zeiss Primovert microscope (Zeiss).

Fourty-eight hours after both transfections the wells or dishes were washed and trypsinized. Culturing medium was added after cells were dislodged from the surface. Cells were centrifuged (Room temperature, 300 G, 5 min.), and pellet resuspended in PBS with 30-40 % FCS. Cells were sorted based on eGFP-expression on a FacsAria2 (BD Biosciences). The Calcium phosphate transfected cells were stained with 7-AAD (Thermo Scientific, Catalog #00-6993-50) for live/dead discrimination.

Doublet discrimination was performed in a FSC-A/FSC-H-plot. Gating of cells was performed in a FCS-A/SSC-A-plot. The FITC-channel was used to sort eGFP-producing cells. The FITC-A gate was set according to the NTC not expected to contain eGFP-producing cells. The sorted cells were collected in a 0,5 ml tube containing PBS with 40% FCS and seeded in a 6-well plate.

2.12 Extraction of genomic DNA from cell lines

Genomic DNA extraction was performed using the Purelink® Genomic DNA kits (Thermo Scientific, Catalog #K1820-01). $2*10^6$ transfected cells were detached and centrifuged for 5 minutes at 300 RCF and 20 °C. Pellets were resuspended in PBS (Gibco, Catalog # 14200-067). The cells were subsequently treated with Proteinase K, RNase A and lysis buffer. Solution containing gDNA was then heated (55 °C) for 10 min. and 96% ethanol was added. The solution with gDNA was incubated on the membrane of a spin column for 3 min and centrifuged. The

column was washed twice by adding two different wash buffers and centrifuging. gDNA was eluted into sterile 1.5-ml microcentrifuge tubes by incubating elution buffer on the membrane of the column and centrifuging. All centrifugation steps were performed at 10-12.000 G. DNA-concentrations and purity ratios of solutions containing the extracted plasmids, were assessed using a DS-11 FX spectrophotometer/Fluorometer (DeNovix). Solutions with a 260/280 nm absorbance ratio close to 1.8 (above 1.6 and below 2.0) as well as a 260/230 nm ratio between 2.0 and 2.2, were considered pure.

2.13 Cripto-1 primer design and validation

A primer pair (listed in Table 2.10) amplifying the third exon on Cripto-1 were generated using the NCBI primer design tool (46). A range was selected allowing primers that generated a 1500bp < size amplicon containing exon 3 from *Cripto-1*. Database used was; *"Refseq representative genomes"*, and organism was set to: *"Homo sapiens"*.

PCR-reaction mixture	**Working volume (50 µl)**	PCR-steps
GC-buffer (5X)	10 µl	1 Cycle – 98 °C (30 seconds)
10 mM dNTP	1 µl (200 µM)	25 Cycle – 98 °C (10 seconds)
Cripto-1 Fw	0,5 µl (0,1 µM)	59 or 65 °C (20 seconds)
Cripto-1 Rw	0,5 µl (0,1 µM)	72 °C (30 seconds)
DMSO	1,5 µl	1 Cycle – 72 (cool to 4 °C)
Template (gDNA)	X µl (50 ng)	(10 minutes)
Phusion hotstart II DNA Polymerase (2 U/µl)	0,5 µl (0,02 U/µl)	
Nuclease-free H_2O	Y µl (up to 50 µl)	

Table 2.13: PCR-reaction mixture, volumes and steps. Denaturation was performed at 98 °C, annealing at 59 or 65 °C and extension at 72 °C using a T100 Thermal cycler (Bio-Rad, catalog # 1861096)

To assess specificity of the primer pair, PCR was performed on gDNA from Hek293T and U87 cells, and the product run on a 1,5 % agarose gel. PCR was performed using the Phusion hotstart II polymerase kit (Thermo Scientific, Catalog # F549L). The PCR-mixture and Thermal cycler settings can be seen in Table 2.13.

2.14 ICE-analysis of amplicons from transfected cells

2.14.1 sgRNA2, sgRNA3 and sgRNA4

Genomic DNA extracted from untransfected and transfected U87 was amplified by PCR (see Table 2.13) and run on 1,5 % agarose gels at 100 v for 25-30 minutes. Gel-bands containing the PCR-

products were cut from the gel with a scalpel. DNA was excised from the gel slices using the Purelink quick gel extraction kit (Thermo Scientific, Catalog#K210012). Briefly the gel slices were mixed with gel solubilization buffer (300 µl pr. 0,1 gram gel) and heated (55 °C) until dissolved. The dissolved gel was incubated on the membrane of a Quick Gel Extraction Column for 3 min. and centrifuged. Wash buffer is added to the membrane and the column is centrifuged again. After a second centrifugation step, the column is transferred to a 1,5 ml tube and elution buffer is incubated on the membrane for 3 min. DNA is eluted into the 1,5 ml tube by centrifugation. All centrifugation steps were carried out at 12.000 G for 1 min. at 20 °C.

Concentration of DNA in the gel-extract and purity ratios were assessed using a DS-11 FX spectrophotometer/Fluorometer (DeNovix). Gel-extract were diluted to a concentration of 5 ng/µl. 15 µl of diluted gel-extract were mixed with 2 µl *Cripto-1 forward* primer (see Table 2.10) and sent to Eurofins genomics labs for sequencing. Sequencing chromatograms from transfected cells were compared with chromatograms of an unedited control (untransfected) in the online tool ICE (8) to assess indel-frequency in the transfected sample.

2.14.2 sgRNA1 and Non-target RNA

Genomic DNA from transfected U87 was amplified by PCR (see Table 2.13) and run on 1,5 % agarose gels at 100 v for 25-30 minutes. The PCR product was purified with the GeneJET PCR purification Kit (Thermo Scientific, Catalog #K0701). Briefly the PCR-product was mixed with an equal volume of Binding buffer and incubated on the membrane of a GeneJET purification column for 3 min. before centrifugation. Wash buffer was added to the columns which were centrifuged again. A second centrifugation step was performed to remove excess wash buffer. 30 µl Preheated Elution buffer (65 °C) was incubated on the membrane of the column, and the PCR-product was eluted into sterile 1,5 ml. tubes by centrifugation. All centrifugation steps were carried out at 12.000 G for 1 min at 20°C. Concentration of DNA in the purified PCR product and purity ratios were assessed using a DS-11 FX spectrophotometer/Fluorometer (DeNovix). PCR-product was diluted to a concentration of 5 ng/µl. 15 µl of diluted PCR-product was mixed with 2 µl *Cripto-1 forward* primer (see Table 2.10) and sent to Eurofins genomics labs for sequencing. Sequencing chromatograms from transfected (with sgRNA1) cells were compared with chromatograms from unedited U87 (transfected with Non-target RNA), in the online tool ICE (8) to assess indel-frequency in the transfected sample.

3. Results

3.1 Verification of CRISPR-Cas9 plasmid vector

To ensure that the correct plasmid was received from addgene, plasmid verification was performed. plasmid verification was performed on PX461 stocks using single and double digests of NotI and XbaI-endonucleases. Based on an assessment, using Snapgene viewer, double-digests of PX461 is expected to cleave the plasmid into a 6117 bp and 3127 bp fragment (see appendix).

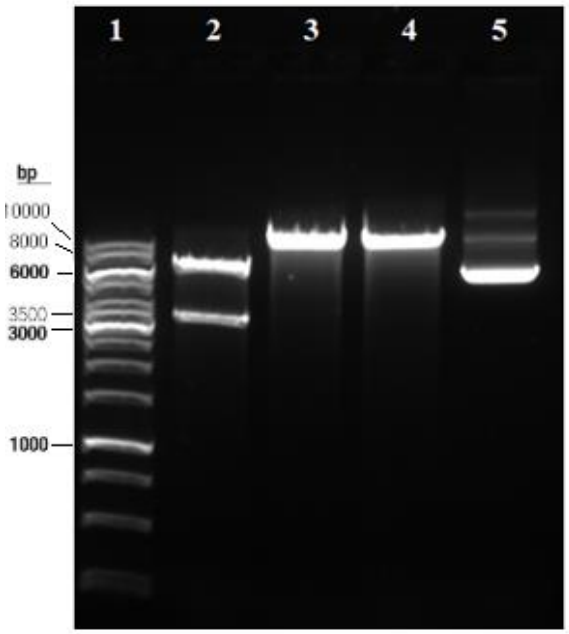

Figure3.1: Digests run on a 1 % agarose gel. Lane 1: 1 Kb ladder. Lane 2: Double (XbaI and Noti) digest. Lane 3: Single digest (NotI) Lane 4: single digest (XbaI) Lane 5: Undigested Plasmid control.

As expected double digestion (Figure3.1 Lane 2) cleaved PX461 into two fragments, a smaller that is located above the 3000 bp-marker, and a larger located slightly above the 6000 bp marker. None of the single digests (Figure3.1 Lane 3, 4) travelled as far as the undigested plasmid control (Figure3.1 Lane 5). This makes sense if the digestion was successful and the single digests are no longer supercoiled. The two fragments on the double digests travelled further than the single digests

3.2 Preparing PX461-vectors with sgRNA-inserts

3.2.1 Design of singleguide-RNA

To identify possible Crispr-guides with targets on exon 3 of *Cripto-1*, the Crispr design tool CrispOr (44)was used. The four sgRNAs with the highest specificity scores were selected (Figure3.1.).

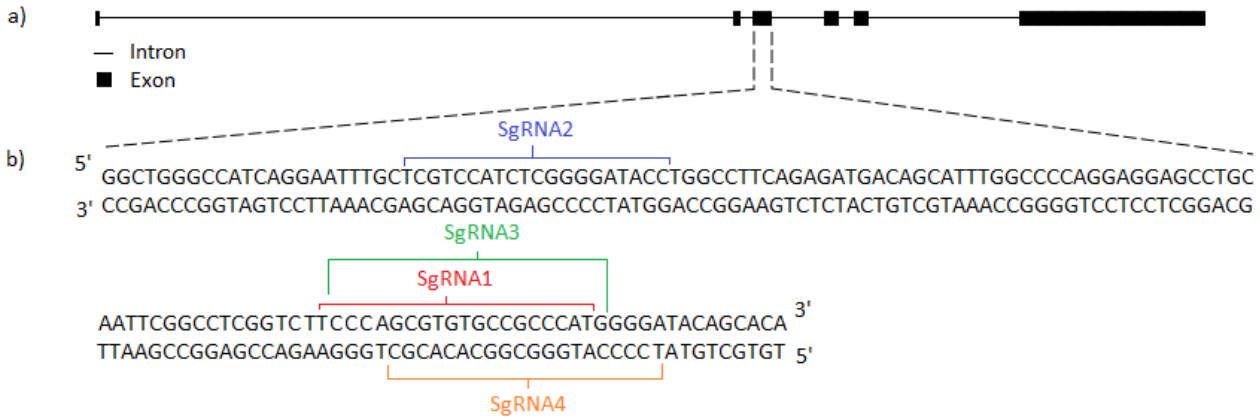

c)

Guide name	Guide sequence	Pam sequence on exon
SgRNA1	5'-TCCCAGCGTGTGCCGCCCAT-*3'*	*GGG*
SgRNA2	5'-TCGTCCATCTCGGGGATACC-*3'*	*TGG*
SgRNA3	5'-CCCAGCGTGTGCCGCCCATG-*3'*	*GGG*
SgRNA4	5'-TCCCCATGGGCGGCACACGC-*3'*	*TGG*

Figure3.2: A) exon-intron structure of the Cripto-1 gene. B) The third exon of Cripto-1 with target-sites of the designed sgRNAs. C) Name of guides, sequences and the Pam sequences preceding the target on exon 3.

3.3.1 Annealing of sgRNA-oligos

The ordered sgRNAs were received as two complementary single-stranded oligos, that needed to be annealed into a duplex before the sgRNA could be integrated into the PX461-vector. To verify that duplex formation had taken place, the annealing product were run on a gel and compared to the sense-strand alone, and the antisense-strand alone (see figure 3.3.1).

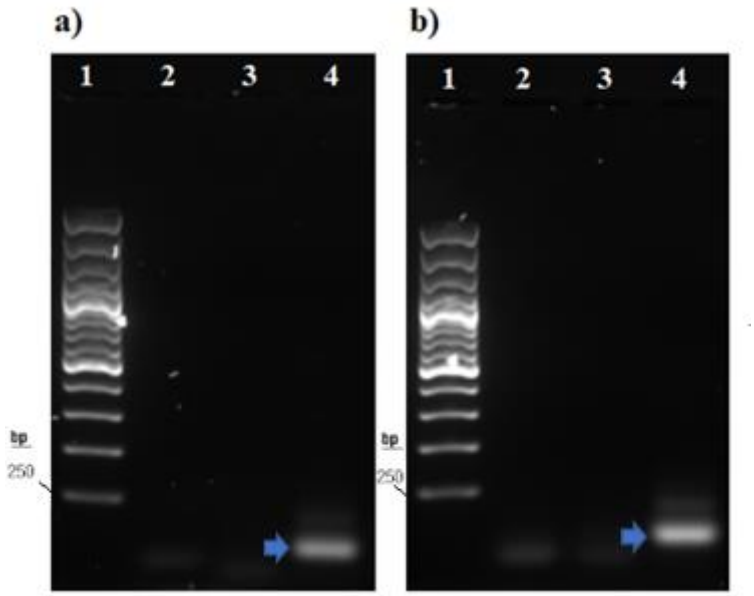

Figure 3.3.1: Method of annealing the sense- and anti-sense strand oligo's were verified using gel-electrophoresis on a 2 % agarose-gel. A) is annealing products from the alpha oligos loaded onto a gel. B) is annealing products from the beta oligos loaded onto a gel. For both gels Lane 1 contains the 1Kb Ladder, Lane 2: the sense strand oligo alone, Lane 3: the anti sense strand oligo alone, Lane 4: are both oligos mixed. Samples in lane 2-4 were treated the same way on the thermocycler prior to gel run (see cloning of PX461 section in methods for more information).

When observing the gels, the brightest bands are located in the lanes loaded with the mixed oligos (figure 3.3.1 marked with blue arrows). This indicates successful annealing of oligos since Gel-red is an intercalating dye and double-stranded DNA, like annealed oligos, should thus appear brighter than bands consisting of single-stranded oligos.

3.3.2 Digestion-ligation of oligos and vector

After successful annealing the oligo-duplexes were ready to be introduced into PX461 plasmids. This was achieved with BbsI-digestion of PX461, and subsequent ligation of annealing product into the vector (methods section 2.7). To assess whether digestion of the plasmids had occurred, digests were run on gels and compared to an undigested PX461-plasmid control.

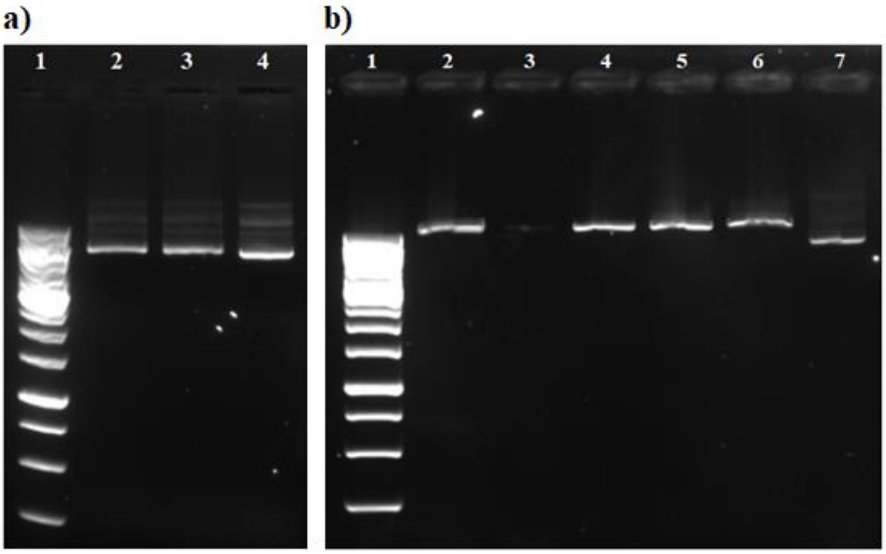

Figure3.3.2a): digestion-ligation products run on a 1 % agarose gel. Lane 1: 1 Kb Ladder. Lane 2: sgRNA2 digestion-ligation product. Lane 3: Non-target digestion-ligation product. Lane 4: Plasmid control
Figure3.3.2b): Digest-ligate products on a 1 % gel. Lane 1: 1 Kb Ladder, Lane 2: beta-digest, Lane 3: empty except for residual Gamma which was loaded in the next well instead. Lane 4: Gamma-digest, Lane 5: delta digest, Lane 6: Scrambled digest, Lane 7: Plasmid control.

As observed in Figure 3.3.2a there was little difference in length travelled on gel between digestion-ligation products in lane 2 and 3 compared to the PX461-plasmid control in lane 4. For this reason, the experiment was repeated with a 50 % increase in volume of BbsI.
As can be seen in Figure3.3.2b the digestion-ligation products (Lane2,4,5,6) did not run as far as the PX461 control (Lane 7), indicating successful cleavage. The new volume of restriction enzyme (1,5 µl BbsI) was therefore used in all subsequent digestion-ligation reactions.

3.4 Design and validation of PX461-sequencing primer

A PX461 primer pair was designed using the Eurofins Sequencing Primer Design Tool. The primer pair amplifies a 527 bp region on PX461 containing the sgRNA insert (if digestion-ligation is successful).

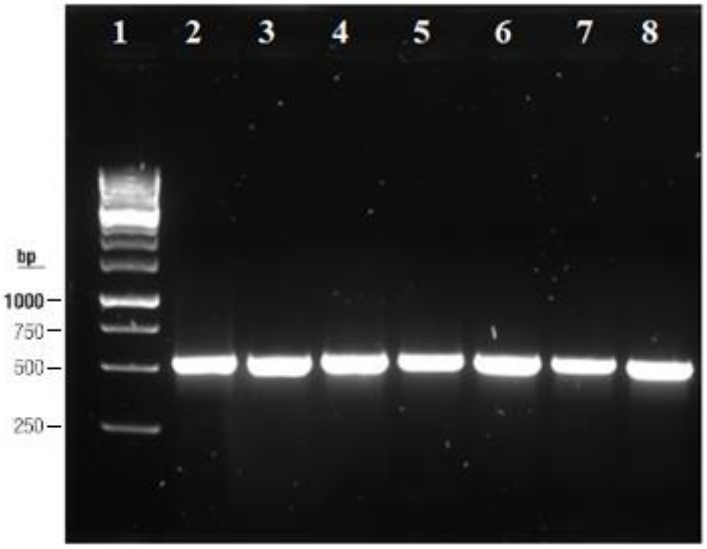

Figure3.4: PCR products of plasmids extracted from transformed bacteria. Run on a 1,5 % gel. Lane 1: 1Kb Ladder, Lane 2,3,4,5,6,7: PCR products using plasmids purified from colonies of transformed bacteria as template. Lane 8: PCR-product using a PX461-control as template. The PX461 primer pair was used as primer for all PCR-reactions.

The PX461 primer pair only generated one band during PCR located slightly above the 500 bp marker which is what we would expect since the amplicon size is predicted to be 527 bp. Since the sequence removed during digestion-ligation is 22 bp, gel-electrophoresis could not be used to identify successfully cloned plasmids since the PCR-products generated from non-inserted and inserted would be the same size.

3.5 Assessment of cloned plasmids by sequencing

The plasmids purified from transformed *E. Coli* were sequenced. The sequencing output was aligned with sgRNA to verify that they were present. As a precaution the returned sequencing output was also aligned with the 22 bp sequence *($5'$CACCGGGTCTTCGAGAAGACCT$3'$)* normally present at the BbsI-cut region to assess whether it had been removed.

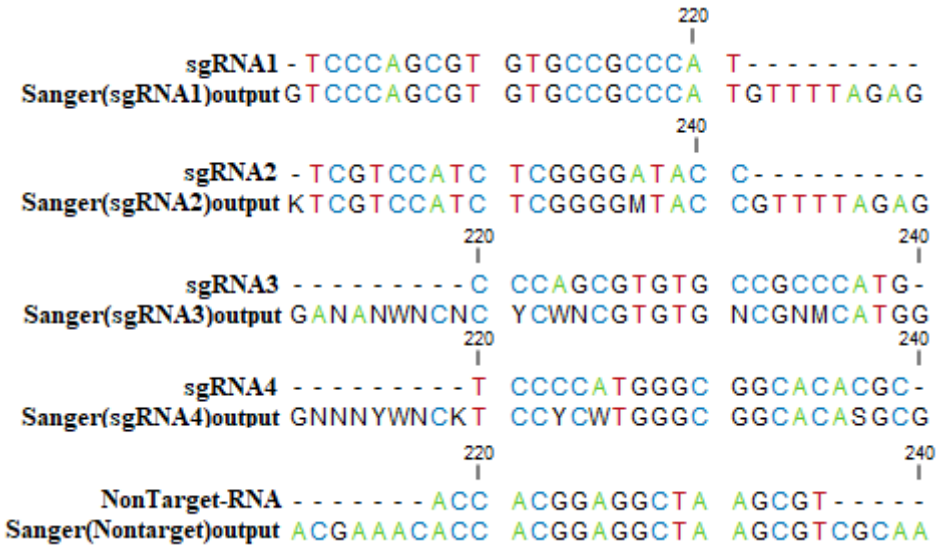

Figure 3.5.1: Alignment between the different sgRNAs (sgRNA1-4 and Non-target-RNA) and the returned sequencing output from the cloned plasmids. A=adenosine, T=Thymine, C= Cytosin, G= Guanine, M= adenosine or Cytosine, N= any base, S= Guanine or Cytosine, Y= Cytosine or Thymine, W= Adenosine or Thymine.

As can be seen in Figure 3.5.1 cloning of the four sgRNAs (and Non-targetRNA) into PX461 was a success since all of them were successfully identified by alignment between sgRNAs and the sequences received from Eurofins.

3.6 Design and validation of the Cripto-1-primer pair

In order to amplify exon 3 of Cripto-1, from gDNA, the Cripto-1 primer pair was designed using the NCBI primer design tool. The PCR-products were run on gels to assess specificity of the primer pair.

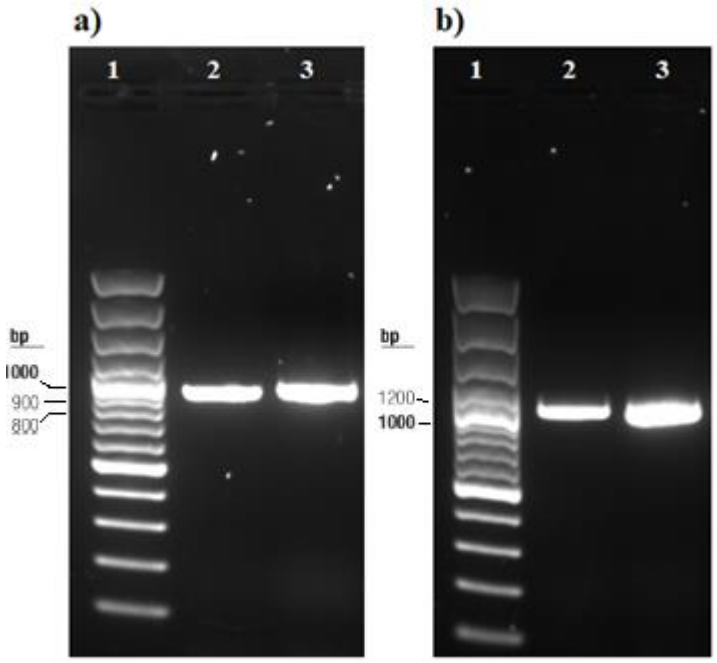

Figure 3.6: A) PCR-product run on a 1,5 % agarose gel. PCR performed with 50 ng genomic DNA template from HEK-293 cells. Lane 1: 100 bp+ Ladder. Lane 2: PCR-product performed with 65° C Annealing temperature. Lane 3: PCR-product, performed with 59 ° C Annealing temperature. B) PCR-product run on a 1,5 % agarose gel. DNA template was 50 ng genomic DNA from U-87. Lane 1: 100 bp+ Ladder. Lane 2: PCR-product performed with an annealing temperature of 65 ° C. Lane 3: PCR-product performed with annealing temperature of 59 ° C.

As can be seen in Figure 3.6, the Cripto-1 primer pair only generated one band, which probably is the amplicon containing exon 3 of Cripto-1.

3.7 Optimization of transfection

Lipofectamine transfection was optimized a total of three times on HEK293T cells, five times on U87 cells, and once on Ntera2-cells to find a setup with sufficient transfection efficiency for later Fluorescence assisted cell sorting. Live/dead assay using Propidium Iodide was performed on four out of five U87 transfections, and all Hek293t transfections. An example of how gating of cells was performed, and how eGFP- and Propidium Iodide-positive cells were identified can be seen in appendix: supplementary Figure 2.

Cell line	Average transfection efficiency (eGFP %)	Average Propidium Iodide % (live dead assay)
U87	4.4 (6.29 if we include EpO-GfP)	2.16
Hek293t	12.1	3.57
Ntera2	6.59	ND*

Figure 3.7: Average Lipofectamine transfection efficiency and Propidium Iodide percentage of U87, Hek293t and Ntera2. ND*- not determined. For U87 a different vector than PX461, named EpO-Gfp was transfected on U87 once. If we include the efficiencies gained by transfecting with EpO-GfP the average efficiency of U87 transfection is raised from 4.4 to 6.29.

As observed in Figure 3.7, Lipofectamine transfection was most effective overall in Hek293t which on average had an efficiency of 12.1 % The efficiency of Ntera2 transfection was roughly half as effective (6.59 %). Transfection of U87 was the least effective overall (4.4 %) Cell death after transfection, as indicated by the propidium Iodide percentage, was 2.16 and 3.57 for U87 and Hek293t respectively. More information about the transfections can be found in Appendix supplementary table 1.

During the fourth Lipofectamine transfection on U87, transfection of an Epo-GFP-plasmid was compared to transfection withPX461. The average efficiency with Epo-GFP was 22.4 %, while the PX461 efficiencies averaged 12.76 % (appendix supplementary table 1).

With Calcium phosphate transfection was performed on U87 twice. While the average transfection efficiency of all wells in the first was 1.15 %, the second transfection achieved an average transfection of 14.46 %, (see Appendix supplementary table 2).

3.8 Fluorescence assisted cell sorting of Lipofectamine transfected U87

Since an optimal transfection efficiency when transfecting U87 could not be achieved with Lipofectamine, several 24-wells transfected and pooled together just prior to the flow-sorting of cells, to gain enough eGFP cells.

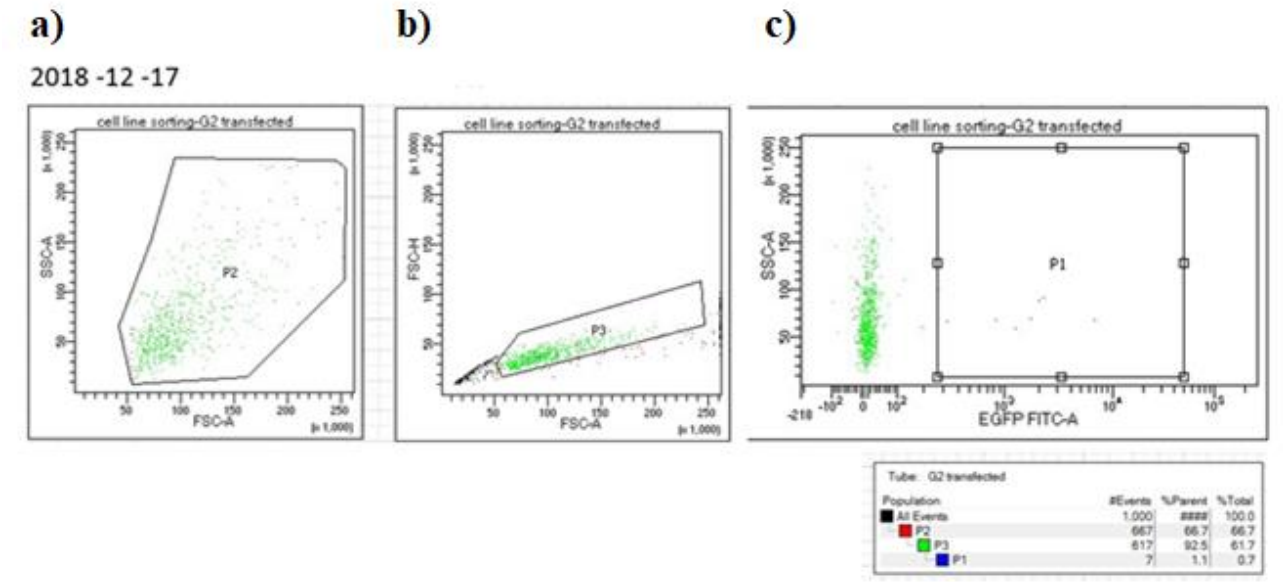

Figure 3.8.1: For flowsorting of sgRNA2,3 and 4 transfected U87, gating of cells was performed in an FCS-A/SSC-A plot(a). Doublet discrimination was performed in an FSC-A/FSC-H plot(b). eGFP-producing cells were sorted using the FITC-A-plot(c). The example shown in the figure is from sgRNA4.

As seen in figure 3.8.1c there we very few events recorded in the eGFP sorting gate (P1). This was the case for all transfections (sgRNA2,3 and 4) even though several 24-wells were pooled together prior to sorting.

Name of transfected sample	Percentage eGFP+ (of gate)	Total cells sorted
sgRNA2	0.1-0.5 %	1800 cells
sgRNA3	0.5-1.3 %	1900 cells
sgRNA4	0.2-0.2 %	700 cells

Table 3.8.2: The 15/12 2018 U87 cells were transfected with sgRNA2,3 and 4 using lipofectamine. The percentage gated cells producing eGFP, as well as total amount of cells sorted are shown here.

As observed in Table 3.8.2 the transfection efficiency ranges from 0.1-1.3 % for the sgRNAs. Less than 2000 cells were sorted for each transfection.

3.9 Sorting of Calcium phosphate transfected U87 and Ntera2

Ntera2 and U87 cells were transfected with Calcium phosphate using the setup that gained the highest efficiency during optimization. The transfected cells were sorted according to eGFP-expression using a Facsaria II.

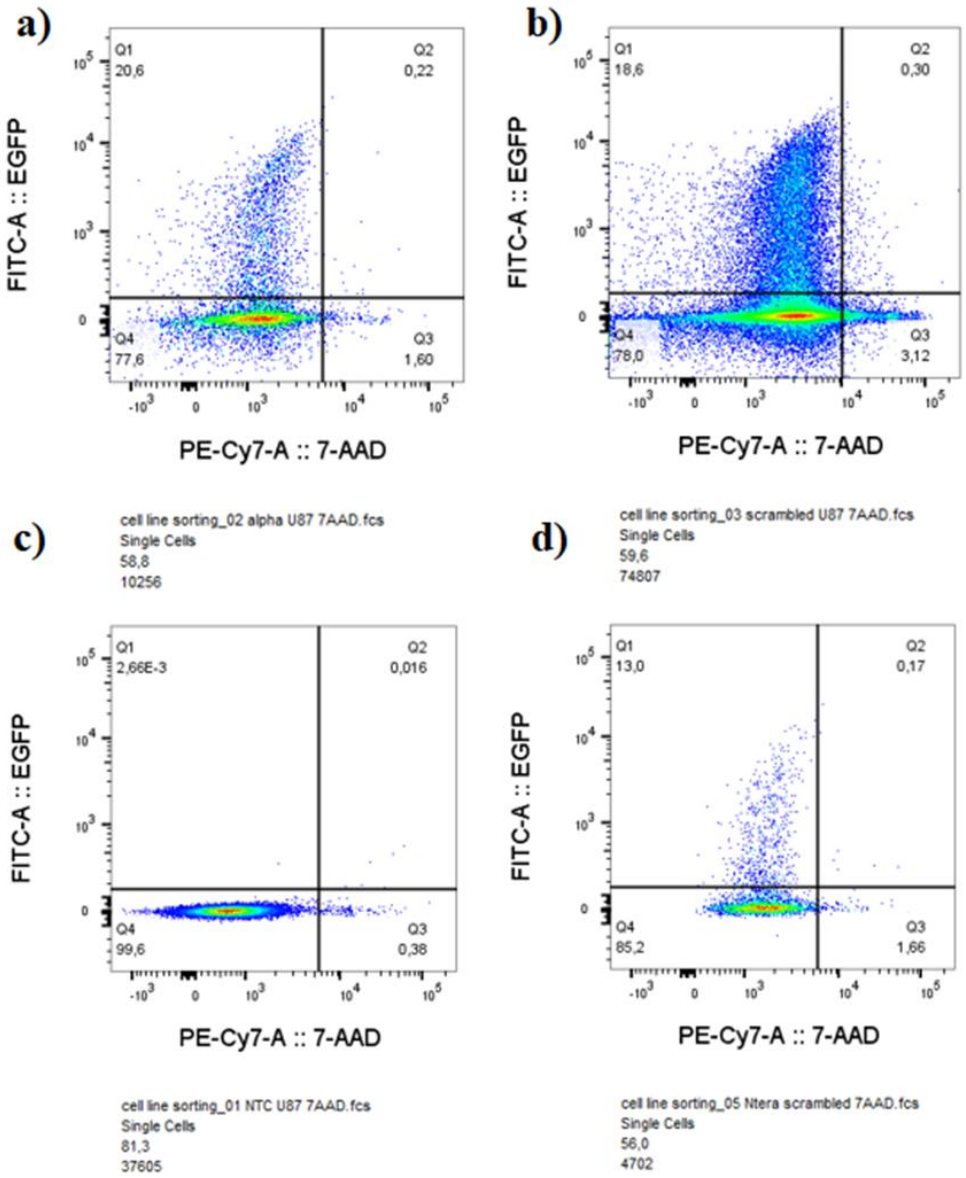

Figure 3.9: The Calcium phosphate transfection performed 2/4 2019 produced efficiencies of 20,6 % (Q1) in the U87 cells transfected with sgRNA1 cloned plasmids (a) which were higher than the previous Calcium phosphate transfections (Supplementary table 2). The efficiency were 18,6 % (Q1) for U87 transfected with Non-target RNA (b). Most gated cells were alive since the eGFP+ (Q2) and eGFP-(Q3) fraction positive for 7-AAD were very low (less than 4 % in the sample with the highest amount of 7-AAD+ events). NTC(c) was used to set the vertical border dividing eGFP+ from eGFP-. Flowsorting of Ntera2(d) For sgRNA1 transfected U87 a total of 24.500 cells were sorted, while for the Non-target transfected, 8.200 cells were sorted

Transfection	Efficiency (eGFP %)	Total cells sorted
sgRNA1	20.61	24.500
Non-target RNA	18.6	8.200

Table 3.9: Efficiency of transfection, and total amount of cells sorted.

As seen in Table 3. transfection efficiencies of 18-6-20.61 % was achieved. Even with these efficiencies, cell amounts were so low that only 24.500(sgRNA1 transfected) and 8.200(Non-target transfected) cells could be isolated. Flow-sorting of Ntera2 could not be completed since too few events were recorded.

3.10 ICE-analysis of amplicons from transfected cells

The online tool ICE was used to assess indel-frequency generated due to transfection of U87 with sgRNA-containing PX461-vectors. Initially the sgRNA1 and Non-target sgRNA had not yet been cloned. The transfections with sgRNA2, sgRNA3 and sgRNA4 were therefore compared to an untreated bulk of U-87 cells rather than a bulk transfected with the non-target RNA. The sgRNA1 transfection was compared to a bulk transfected with Non-target RNA to assess ICE-score.

Figure 3.11: Summary of results generated by ICE-analysis of sgRNA1 sgRNA2, sgRNA3 and sgRNA4. The four most frequent Indels (or no indels=0) found in the edited samples are shown in the boxes. The ICE-score represent the editing efficiency, namely the percentage of the edited sample that differ from the unedited control. The r^2 score is the Pearson correlation coefficient(r) representing how confident we can be in the ICE-score. The knockout (KO)-score is a measure of the proportion of cells from the edited sample with either a frameshift or a 21+ bp indel.

For sgRNA2, 3 and 4 transfected cells indels were introduced in about 3-4 % of cells according to the ICE-scores (Figure 3.11). Virtually all the indels generated in the sgRNA2 and sgRNA3 bulk of cells, are likely to have resulted in a KO since the ICE and KO-score is similar for these samples.

When comparing the ICE and KO-score for the sgRNA4-transfected bulk of cells 75 % of indels generated are likely to result in knockout of Cripto-1.

For sgRNA1 the ICE-score shows that indels were generated in about 20 % of the U87 cells transfected with sgRNA1. Out of all transfected cells 18 % contained an indel likely to result in knockout of Cripto-1 (Figure 3.9) based on the KO-score. When comparing the ICE- and KO-score 90 % of all indels generated are thus likely to cause Cripto-1 knockout.

4. Discussion

4.1 CRISPR Cas9 vs RNAi, ZFN and TALEN

In this study the CRISPR Cas9 system was used for knocking out Cripto-1 in U87-cells. However other knockout/knockdown methods are available for suppression of gene-expression, so why was CRISPR Cas9 chosen for this study? One alternative method is RNA interference (RNAi) (introduction section 1.7). Unlike CRISPR Cas9 knockout which requires introduction of Cas9-endonucleases (either directly or as plasmids encoding Cas9) RNAi relies on the RNA-induced silencing complexes (RISCs) already present in mammalian cells. With RNAi the lengthy process of cloning sgRNAs into plasmids and verification with sequencing, could thus have been avoided, since all we would need is siRNA complementary to Cripto-1 mRNA (30).

One important feature of RNAi is that it introduces knockdown rather than knockout. Knockdown by RNAi may mRNA levels of a gene, but the protein can still be produced at low levels (30). It is possible to reduce the protein levels substantially with RNAi. A team of researchers investigating the effect of ribonucleotide reductase subunit-2 (RRM2) was able to reduce the RRM2 protein content with 90 % using RNAi (47). However even with high reduction of protein product, the CRISPR Cas9 system is more convenient since it causes knockout at the genetic level, and thus disrupts the ability of cells to even produce the protein product. Given enough time protein-products should eventually be depleted from knockout cells. This eliminates low concentrations of the protein as a confounding factor when results need to be interpreted. (30) For these reasons CRISPR Cas9 a more attractive tool for assessing the role of Cripto-1 in GBM (48).

Permanent knockout via introduction of DBs can also achieved with the gene-editing tool ZFN and TALEN (introduction section 1.7) However, CRISPR Cas9 does have an important advantage over ZFN and TALEN, namely its simplicity. It is much easier to design CRISPR-Cas9 complexes specific towards its desired target, since it only requires alteration of the 20 bp sequence of the guide RNA whereas ZFN and TALEN requires changes in order of 500-1500 bps in protein-coding sequences when preparing complexes with sufficient affinity towards its genomic target (32). Since preparing gene-editing with CRISPR can be achieved in a less labor-intensive manner, it is simply a more convenient tool than ZFN and TALEN for knocking out Cripto-1 in GBM.

4.3 Stable vs. Transient expression

One thing that needs to be considered is whether CRISPR Cas9 plasmid vector should be expressed transiently or stably in U87? Stable expression is achieved when the transfected DNA is integrated

in the host cells genome, leading to long term expression. With transient expression the transfected genetic material is not integrated and only present temporarily in the cell (49) (50). Stable expression can be induced for instance by lentiviral delivery of CRISPR Cas9 genes (51), while transient can be induced by delivery of plasmids, mRNA encoding Cas9 and purified Cas9 Ribonucleoproteins (RNPs) into cells (52). At first it may seem like an advantage to choose a stable expression approach to ensure Cas9 is expressed long enough for successful editing. However, a study comparing three transient approaches demonstrates that longer expression of Cas9 does not necessarily equal higher indel-frequency. In the study Liang et. al. transfected HEK293FT cells with Cas9-Plasmids, mRNA encoding Cas9 and Cas9-proteins, targeting three different loci. The three approaches cleaved their target with equal efficiency at 24 hours and maintained a high efficiency 48-72 hours after transfection. While the efficiency was similar western blotting revealed that Cas9-plasmid transfection resulted in sustained presence of Cas9-proteins even after 72 hours. The Cas9-protein was depleted quicker with Cas9-mRNA transfection but lasted longer than the Cas9-protein approach, in which Cas9-proteins decreased rapidly after 4 hours. (52)

Liang et. al. decided to test whether the rapid removal of Cas9-proteins observed with the protein- and mRNA-transfection approach would resulted in fewer off-targets than with the plasmid-transfection approach. By assessing two genomic sites, deemed to be at high risk of off-targeting, they discovered that plasmid transfection produced more off-target indels than Cas9-mRNA and Cas9-protein transfection (52). We do not know for sure whether the plasmid transfection overall produced more off-target indels since Liang et. al. only tested two loci, and CRISPR has been demonstrated before to cleave sites with several mismatches with just as high frequencies as their intended target (53). The results by Liang et. al. suggests that variations of Cas9-protein concentrations, even within 48-72 hours post-transfection, can impact degree of off-targeting. The same thing was observed in a study by Kim et. al. where Cas9-Ribonucleoproteins (RNPs) and CRISPR-Cas9 plasmids were transfected into K562-cells. It was observed that Cas9-protein concentration were reduced rapidly in cells transfected with RNPs compared to plasmids. RNPs were better able to avoid mutating two genomic sites that only differed by 2 nucleotides from the intended target, compared to plasmid transfection. The reduced off-targeting with RNP-transfection were attributed to the rapid degradation of the RNP's (54). In yet another study direct Cas9-protein transfection was compared to Cas9-plasmid delivery and turned out to be more than ten times as specific. The authors believed this was likely due to the short amount of time Cas9-proteins would be active in the cells with Cas9-protein transfection, compared to plasmid transfection (55).

In summary prolonged expression of Cas9-nucleases does not necessarily enhance editing efficiency and seems to correlate with an increase in off-targeting. Since increased off-targeting can be observed even in transient approaches with prolonged presence of Cas9 compared to transient approaches with shorter windows of Cas9-nuclease activity, a long term stable approach does not seem preferable to a transient approach. For this reason, a transient expression was used in this study.

4.4 Cloning of PX461

Cloning of the four sgRNAs and the non-target RNA eventually succeeded and was verified by sequencing. Prior to success however there were some complications. The plasmids used during digestion-ligation sometimes appeared too similar to untreated plasmid controls on gels (Results section 3.3.2 Figure 3.3.2a), and the concentration of enzymes (BbsI and ligases) had to be adjusted until visual differences (like shorter distance travelled on gel since it is not supercoiled after cleavage) between digest-ligates and controls were observed (Results section 3.3 figure 3.3.2B). Even after this the ligation-products still contained PX461 without integrated sgRNAs as evidenced by sequencing of plasmids extracted from some colonies (see appendix), and experiments had to be repeated. Although cloning eventually was a success the question remains whether a different method, than restriction-ligation based cloning would have resulted in fewer complications. It is unknown whether any of the negative results is due to inefficient ligation, but lack of digestion was certainly a source of some problems (results, section 3.3.2 Figure 3.3.2a). A cloning method that does not rely on restriction cleavage might therefore be preferable.

One alternative method would be the In Fusion cloning method. This cloning method exploits the ability of the In Fusion Enzyme to fuse 15 bp homologous regions. Preparing cloning with this method can be a bit complicated in its primer design but requires no restriction or ligation enzymes. Once primers have been designed only three PCR-reactions are needed and the amplicons can simply be mixed and fused with the In Fusion enzyme (56).

Another possible alternative would be TOPO-cloning which requires a linearized vector with viral topoisomerase attached, as well as PCR amplification of the insert (using Taq-polymerase). After mixing the amplified insert and Vector, the insert is introduced by the topoisomerase. In practice this means that no addition of restriction enzyme is necessary, and ligation is carried out by the attached topoisomerase. (57) (58)

During the digestion ligation reaction in this study, there were 6 cycles alternating between the optimum temperature of restriction cleavage (37 °C) and ligation (23 °C)(Methods section 2.7). Since plasmids initially appeared to be undigested (results, section 3.3.2 Figure 3.3.2a) one possible adjustment besides the increase in restriction enzyme concentration, would have been prolongation of the restriction cleavage step with 37 °C. With TOPO-cloning however no optimization of concentration of enzymes would be necessary, nor optimization of duration of reaction temperatures. With TOPO-cloning only one enzyme already present with the vector is used, and thus only one optimum temperature is necessary, making TOPO-cloning is simpler-to-perform alternative to restriction cloning with fewer parameters to adjust. (57) (58)

4.5 Why were the ICE-Scores so low?

The ICE-scores showed that indels were introduced in less than 5 % of U87 cells transfected with sgRNA2, sgRNA3 and sgRNA4 using lipofectamine. The sgRNA1 Calcium phosphate-transfection, introduced indels in 20% of cells of which 90 % are expected to be knockout cells based on the comparison of the ICE- and KO-score. The difference in ICE-score is most likely due to the observed differences in transfection efficiency. Prior to sorting of U87, preparation using Calcium phosphate transfection resulted in efficiencies of 20.6 % and 18.6 % for sgRNA1 and Non-targetRNA respectively. (Results section 3.9). This was superior to the lipofectamine transfections which resulted in efficiencies as low as 0.1-1.3 % for sgRNA2,3 and 4 (results section 3.8).

4.6 Optimizing Transfection efficiency

To find the optimal setup, with lipofectamine, that would produce transfection efficiencies sufficiently high for sorting, different amounts of DNA(PX461), P3000 and L3000 reagents were tested (see appendix, supplementary table 1). Testing different combinations on U87 five times the efficiency averaged 4.4 % (Results section 3.7 Figure 3.7). Transfection of Ntera2 was performed once with an average efficiency of 6.59 % out of 8 wells. Hek293t was transfected three times with an average efficiency of 12.1 % Only rarely did the efficiency of U87 transfection exceed 10 %, and even when it did the success could not be replicated when transfecting in preparation for FACS which yielded efficiencies between 0.1-1.3 % (Results section 3.8). Why were the transfection efficiencies consistently low with lipofectamine and how can it be improved? One possibility would be to use a smaller Cas9-plasmid than PX461. A previous study investigated the relationship between plasmid DNA size and transfection efficiency, when DNA were delivered as lipoplexes into HeLa cells. The results showed that transfection efficiency was greater with smaller plasmids than with larger, as assessed by luciferase activity of HeLa cells transfected with 3700-, 8600- and

19 600 bp sized plasmids (59). Likewise, in this present study the effect of plasmid size on efficiency was investigated during the fourth lipofectamine transfection (Appendix: Supplementary Table 1) (Results section 3.7). The PX461 was compared to an Epo-GFP plasmid, used previously by Burkhart et. al. which was smaller (6703 bp vs. 9288 bp) than PX461 (60). Using the same setup, the efficiencies when transfecting U87 with Epo-GFP averaged 22.4 %, while the PX461 efficiencies averaged 12.76 %. (Results section 3.7). Based on that experiment alone a smaller plasmid would appear a better choice, since no Lipofectamine transfection with PX461 ever reached the efficiencies of EpO-GfP on U87 (Results section 3.7) (Appendix: Supplementary Table 1).

In addition to transfecting with smaller plasmids, it may also be possible to increase efficiency by switching to another GBM cell line. In this study Lipofectamine-transfection was attempted on Ntera2 once, and Hek293T cells three times. Transfection of eight wells with Ntera2 resulted in an average efficiency of 6.59%, while the average efficiency of the HEK293T transfections is 12.1 % (Results section 3.7) Which were both higher than U87 (average 4.4%). Since HEK293T are known to be easy to transfect, it is not surprising that higher efficiencies were gained with this cell line (61). Even among cell lines belonging to the same form of cancer, variations in transfection efficiencies are observed. An example of this is seen in one study by Hagemann et. al. where three glioblastoma cell lines (U373, U251 and GaMG) were transfected using the same lipofectamine setup. Lipofectamine transfection of U373, U251 and GaMG yielded efficiencies of 18 %, 20 % and 4 % respectively (62).

With Calcium phosphate transfection a setup with average efficiencies of 14,46 % was achieved after just two optimizations (Results section 3.7). The relatively high efficiency was reproducible when preparing for sorting, (18, and 20, % efficiency) (Results section 3.9) unlike lipofectamine (Results section 3.8). One drawback of Calcium phosphate was its apparent cytotoxicity. The NTCs of both U87 and Ntera2 looked healthy with an increase in confluency 24-48 hours post-transfection, the Calcium phosphate transfected U87 and Ntera2 experienced a large decrease in confluency 24-48 post-transfection (Appendix: Supplementary Figure 4, 5). This might explain why only 8.000 and 24.500 U87 cells could be sorted into a bulk of eGFP-cells, and why there were too few eGFP-producing cells among Ntera2 for flowsorting (since almost no Ntera2 were alive 48-hours after transfection as seen in Figure 5). Propidium Iodide-staining showed that on average 3.57% of HEK293t-cells were dead after Lipofectamine transfection. The average Propidium Iodide measurement on U87 transfected with lipofectamine were 2.16. (Results section 3.7). Based on this Lipofectamine, unlike Calcium phosphate, does not seem very cytotoxic. However, the low

Propidium Iodide is probably due to the generally low transfection efficiency (Results section 3.7). Calcium precipitates are cytotoxic which propably is the reason for the observed reduction in cell content of transfected wells (63) (Appendix: supplementary Figure 3 and 4). Given the low efficiency of Lipofectamine and cytotoxicity of Calcium phosphate, the question is whether lipofectamine and Calcium phosphate really is the most suitable transfection method for U87, or whether alternatives should be considered.

In our study the highest transfection efficiencies on U87 were achieved with Calcium phosphate. Calcium phosphate has been compared to Lipofectamine before, in the 1321N1-astrocytoma cell line, and found to be slightly inferior. Repeated optimization of both methods resulted in transfection efficiencies as high as 40 % with calcium phosphate and 50 % with Lipofectamine. (64) Liposomal transfection of GBM-cells has been performed previously on U118-MG glioblastoma and rat C6 glioma cell lines with transfection efficiencies reaching 33-36 % (65). The study by Hagemann et. al. that transfected the U373, U251 and GaMG GBM cell lines with lipofectamine also performed Nucleofection transfection on the same cells and compared their efficiencies with those of Lipofectamine. Nucleofection is a transfection technique in which DNA is introduced into cells through pores in their membrane generated by electroporation. With nucleofection an efficiency of 71 %, 96% and 83 % were gained for U373, U251 and GaMG respectively (depending on which nucleofector solution they used). Based on those results Hagemann et. al. regarded lipofection as inferior to nucleofection (at least when transfecting the three GBM cell lines). (62)

It should be noted that the high transfection efficiencies with nucleofection was generated by Hagemann et. al. as a result of intense optimization with several programs and three different nucleofector solutions tested. The lipofectamine transfection appear to have been performed only once with no further optimization since the authors stated that they simply multiplied the values from invitrogen's protocol to fit a 6-well format. Moreover, efficiencies with nucleofection ranged from anywhere between 0,8-95,7 % during the optimization. If the authors had optimized the lipofectamine transfection as vigorously as they had with nucleofection, the comparison might have turned out very different. (62) It is thus unclear whether nucleofection really is more effective towards the selected GBM cell lines, than lipofectamine, but Hagemann et. al. certainly demonstrated that nucleofection can effectively transfect them. (62).

Nucleofection, unlike lipofectamine and calcium phosphate, does not depend on cell division for transfected DNA to reach the nucleus, since DNA is bound to proteins that promote active transport

into the nucleus. This is an advantage when transfecting quiescent or slowly dividing cells (62) (66). The U87 line employed here however had a steady growth rate (observe difference in confluence between day one and two after Calcium Phosphate transfection in NTC in appendix: Supplementary Figure 4), which ought to have provided DNA, transfected with lipofectamine and calcium phosphate, ample opportunity to enter the nucleus. Lack of growth is thus probably not the reason for transfection failure. One drawback of electroporation-based techniques like nucleofection is the number of parameters, like voltage and pulse duration, that can be adjusted. Optimization is much more complicated than lipofectamine and calcium phosphate, which is rather straightforward (amount of DNA and reagent used and others). This drawback however can be an advantage when dealing with cell lines that are otherwise difficult to transfect, since the electrical parameters can be adjusted to suit the cell of interest. With electroporation even transfection of lymphocytes, which cannot properly be transfected with Calcium phosphate, is possible. (62) (67) It should also be noted that while Hagemann et. al. tested 30 different combinations of electrical parameters and solutions on U251 the viability was above 93 % in 17 cases (and above 90 % in 23 cases) of the setups, indicating that optimal viability of transfected cells can be achieved at least in this GBM cell line. (62) It would be interesting to compare Calcium phosphate and nucleofection on U87 to see which technique can achieve the highest transfection efficiency while maintaining a high cell viability. In summary while Lipofectamine has and Calcium phosphate has produced disappointing results in our U87 cells, electroporation-based techniques, such as nucleofection, is a promising tool that might be worth the cumbersome optimization process in GBM cell lines like U87.

4.7 Cripto-1 and invasiveness in cancer

Regardless of which method used for preparing knockout/knockdown, silencing of Cripto-1 in different cancers has so far proven useful in studying tumor migration and invasiveness. An example, by Liu et. al. was given in the introduction (section 1.6) in which a malignant prostate cancer cell (PCCs) line was treated with silencing RNA (siRNA) against Cripto-1. The knockdown of Cripto-1 decreased the migration of cells in a wound healing assay and reduced invasion in a transwell assay. Additionally, β-catenin was found downregulated, while E-cadherin (a marker lost during EMT) was upregulated once Cripto-1 was knocked down by siRNA. Due to these findings Liu et. al. believed that Cripto-1 regulated EMT through the Wnt/β-catenin pathway in PCCs. (28) Another study investigated the role of Cripto-1 in nasopharyngeal carcinoma cells (NPCs) by introducing stable expression of RNA interfering Cripto-1. Knockdown of Cripto-1 resulted in reduced invasion in a boyden-chamber assay (29).

Few studies have investigated the role of Cripto-1 in GBM. The degree of Cripto-1 expression in GBM-tissue from patients has been assessed by Pilgaard. et. al. (68) and Tysness et. al. (69), and recently the effects of overexpressing Cripto-1 in GBM has been studied (70). Since the role of Cripto-1, in various cancers, has been successfully elucidated in previous knockdown studies (28) (29), it would be interesting to use the cloned plasmids in this study to investigate the role of Cripto-1 in GBM invasiveness and migration.

4.8 Future setup and perspectives

To assess the role of Cripto-1 in migration and invasion of GBM we need a monoculture of knockout-Cripto-1 U87 that can be compared with wildtype U87. We also need a U87-cell line with induced overexpression of Cripto-1 like in a previous study (71). To get a knockout culture we need a bulk of transfected and sorted cells from which we can distribute single cells in wells (either by limiting dilution or with a flow sorter). The KO-score should preferably be >33 % so we can expect to find knock-out cultures without having to grow too many of them from single sorted cells. As the cultures grow they will be split into progressively larger wells/flasks until knockout of Cripto-1 in monocultures can be verified using immunofluorescence microscopy, q-PCR, western blotting and sanger sequencing. Once knockout has been confirmed, and once we have a Cripto-1 overexpressing, a wildtype and a knockout cell line we can perform in vitro migration assays by growing tumorspheres of each cell line on Geltrex matrix and monitor migration daily in a microscope (72). Whether or not Cripto-1 is important for migration can be assessed by comparing the growth rate between the three cell lines (72). Differences in invasive capabilities of Cripto-1 knockout, wildtype and an overexpressing GBM phenotype can be compared in a boyden chamber assay with 10 % serum in a bottom chamber as performed previously (29). Once migration and invasion has been assessed in vitro, an in vivo Xenograft assay can be performed. In this assay GMB-tumor spheres are injected into the brain (at striatum) of mice. Subsequent Immunofluorescence analysis against markers of EMT (which transitions cells into a more migratory phenotype as well as invasive CSCs) can be performed on excised CNS-tissue containing GBM-tumor. If knockout of Cripto-1 substantially reduces migration and invasion effects in GBM, Cripto-1 could perhaps be a possible therapeutic target in this form of cancer.

5. Conclusion

The four sgRNA's targeting Cripto-1 and the Non-target RNA were successfully cloned into PX461-vectors. Indels expected to generate knockout was achieved in up to 18% of U87.

Restriction-based cloning was an effective method for introducing sgRNA into the PX461-vector

Lipofectamine transfection was an inferior method in terms of transfection efficiency of U87, while Calcium phosphate was inferior in terms of cell viability of U87.

6. References

1. Urbańska K, Sokołowska J, Szmidt M, Sysa P. Review Glioblastoma multiforme – an overview. Współczesna Onkol [Internet]. 2014 [cited 2019 May 25];5(5):307–12. Available from: http://www.ncbi.nlm.nih.gov/pubmed/25477751
2. Louis DN, Perry A, Reifenberger G, von Deimling A, Figarella-Branger D, Cavenee WK, et al. The 2016 World Health Organization Classification of Tumors of the Central Nervous System: a summary. Acta Neuropathol [Internet]. 2016 Jun 9;131(6):803–20. Available from: http://link.springer.com/10.1007/s00401-016-1545-1
3. Walid MS. Prognostic factors for long-term survival after glioblastoma. Perm J [Internet]. 2008 [cited 2019 May 25];12(4):45–8. Available from: http://www.ncbi.nlm.nih.gov/pubmed/21339920
4. Tomiyama A, Ichimura K. Signal transduction pathways and resistance to targeted therapies in glioma. Semin Cancer Biol [Internet]. 2019 Jan 24 [cited 2019 May 25]; Available from: https://www.sciencedirect.com/science/article/pii/S1044579X18300981
5. Stupp R, Mason WP, van den Bent MJ, Weller M, Fisher B, Taphoorn MJB, et al. Radiotherapy plus Concomitant and Adjuvant Temozolomide for Glioblastoma. N Engl J Med [Internet]. 2005 Mar 10 [cited 2019 May 25];352(10):987–96. Available from: http://www.nejm.org/doi/abs/10.1056/NEJMoa043330
6. Lathia JD, Mack SC, Mulkearns-Hubert EE, Valentim CLL, Rich JN. Cancer stem cells in glioblastoma. Genes Dev [Internet]. 2015 Jun 15 [cited 2019 May 25];29(12):1203–17. Available from: http://www.ncbi.nlm.nih.gov/pubmed/26109046
7. Erasimus H, Gobin M, Niclou S, Van Dyck E. DNA repair mechanisms and their clinical impact in glioblastoma. Mutat Res Mutat Res [Internet]. 2016 Jul 1 [cited 2019 May 25];769:19–35. Available from: https://www.sciencedirect.com/science/article/pii/S1383574216300151
8. Hatoum A, Mohammed R, Zakieh O. The unique invasiveness of glioblastoma and possible drug targets on extracellular matrix. Cancer Manag Res [Internet]. 2019 Feb [cited 2019 May 25];11:1843–55. Available from: http://www.ncbi.nlm.nih.gov/pubmed/30881112
9. Rangel MC, Karasawa H, Castro NP, Nagaoka T, Salomon DS, Bianco C. Role of Cripto-1 during Epithelial-to-Mesenchymal Transition in Development and Cancer. Am J Pathol

[Internet]. 2012 Jun 1 [cited 2019 May 25];180(6):2188–200. Available from: https://www.sciencedirect.com/science/article/pii/S000294401200257X

10. Catalano M, D'Alessandro G, Lepore F, Corazzari M, Caldarola S, Valacca C, et al. Autophagy induction impairs migration and invasion by reversing EMT in glioblastoma cells. Mol Oncol [Internet]. 2015 Oct 1 [cited 2019 May 29];9(8):1612–25. Available from: http://doi.wiley.com/10.1016/j.molonc.2015.04.016

11. Beier D, Hau P, Proescholdt M, Lohmeier A, Wischhusen J, Oefner PJ, et al. CD133+ and CD133- Glioblastoma-Derived Cancer Stem Cells Show Differential Growth Characteristics and Molecular Profiles. Cancer Res [Internet]. 2007 Apr 24 [cited 2019 May 29];67(9):4010–5. Available from: http://www.ncbi.nlm.nih.gov/pubmed/17483311

12. Velpula KK, Dasari VR, Tsung AJ, Dinh DH, Rao JS. Cord blood stem cells revert glioma stem cell EMT by down regulating transcriptional activation of Sox2 and Twist1. Oncotarget [Internet]. 2011 Dec [cited 2019 May 29];2(12):1028–42. Available from: http://www.ncbi.nlm.nih.gov/pubmed/22184289

13. Mani SA, Guo W, Liao M-J, Eaton EN, Ayyanan A, Zhou AY, et al. The Epithelial-Mesenchymal Transition Generates Cells with Properties of Stem Cells. Cell [Internet]. 2008 May 16 [cited 2019 May 29];133(4):704–15. Available from: https://www.sciencedirect.com/science/article/pii/S0092867408004443

14. Cheng L, Wu Q, Guryanova OA, Huang Z, Huang Q, Rich JN, et al. Elevated invasive potential of glioblastoma stem cells. Biochem Biophys Res Commun [Internet]. 2011 Mar 25 [cited 2019 May 29];406(4):643–8. Available from: https://www.sciencedirect.com/science/article/pii/S0006291X11003421

15. Moustakas A, Heldin C-H. Signaling networks guiding epithelial?mesenchymal transitions during embryogenesis and cancer progression. Cancer Sci [Internet]. 2007 Oct 1 [cited 2019 May 29];98(10):1512–20. Available from: http://doi.wiley.com/10.1111/j.1349-7006.2007.00550.x

16. Lo RC-L, Leung CO-N, Chan KK-S, Ho DW-H, Wong C-M, Lee TK-W, et al. Cripto-1 contributes to stemness in hepatocellular carcinoma by stabilizing Dishevelled-3 and activating Wnt/β-catenin pathway. Cell Death Differ [Internet]. 2018 Aug 14 [cited 2019 May 25];25(8):1426–41. Available from: http://www.nature.com/articles/s41418-018-0059-x

17. Jiang Y-G, Luo Y, He D, Li X, Zhang L, Peng T, et al. Role of Wnt/β-catenin signaling pathway in epithelial-mesenchymal transition of human prostate cancer induced by hypoxia-inducible factor-1α. Int J Urol [Internet]. 2007 Nov 1 [cited 2019 May 29];14(11):1034–9. Available from: http://doi.wiley.com/10.1111/j.1442-2042.2007.01866.x

18. Scognamiglio B, Baldassarre G, Cassano C, Tucci M, Montuori N, Dono R, et al. Assignment of human teratocarcinoma derived growth factor (TDGF) sequences to chromosomes 2q37, 3q22, 6p25 and 19q13.1. Cytogenet Genome Res [Internet]. 1999 [cited 2019 May 30];84(3–4):220–4. Available from: http://www.ncbi.nlm.nih.gov/pubmed/10393436

19. Watanabe K, Bianco C, Strizzi L, Hamada S, Mancino M, Bailly V, et al. Growth Factor Induction of Cripto-1 Shedding by Glycosylphosphatidylinositol-Phospholipase D and Enhancement of Endothelial Cell Migration. J Biol Chem [Internet]. 2007 Oct 26 [cited 2018

Oct 2];282(43):31643–55. Available from: http://www.ncbi.nlm.nih.gov/pubmed/17720976

20. Bianco C, Salomon DS. Targeting the embryonic gene Cripto-1 in cancer and beyond. Expert Opin Ther Pat [Internet]. 2010 Dec 13 [cited 2018 Oct 2];20(12):1739–49. Available from: http://www.ncbi.nlm.nih.gov/pubmed/21073352

21. Rangel MC, Castro NP, Karasawa H, Nagaoka T, Salomon DS, Bianco C. Cripto-1: A Common Embryonic Stem Cell and Cancer Cell Marker. In: Stem Cells and Cancer Stem Cells, Volume 2 [Internet]. Dordrecht: Springer Netherlands; 2012 [cited 2019 May 25]. p. 155–66. Available from: http://link.springer.com/10.1007/978-94-007-2016-9_17

22. Bianco C, Strizzi L, Ebert A, Chang C, Rehman A, Normanno N, et al. Role of Human Cripto-1 in Tumor Angiogenesis. JNCI J Natl Cancer Inst [Internet]. 2005 Jan 19 [cited 2019 May 25];97(2):132–41. Available from: https://academic.oup.com/jnci/article-lookup/doi/10.1093/jnci/dji011

23. Nagaoka T, Karasawa H, Turbyville T, Rangel M-C, Castro NP, Gonzales M, et al. Cripto-1 enhances the canonical Wnt/β-catenin signaling pathway by binding to LRP5 and LRP6 co-receptors. Cell Signal [Internet]. 2013 Jan 1 [cited 2019 May 25];25(1):178–89. Available from: https://www.sciencedirect.com/science/article/pii/S0898656812002665

24. Bao X, Song H, Chen Z, Tang X. Wnt3a promotes epithelial-mesenchymal transition, migration, and proliferation of lens epithelial cells. Mol Vis [Internet]. 2012 [cited 2019 May 29];18:1983–90. Available from: http://www.ncbi.nlm.nih.gov/pubmed/22876125

25. De Silva T, Ye G, Liang Y-Y, Fu G, Xu G, Peng C. Nodal Promotes Glioblastoma Cell Growth. Front Endocrinol (Lausanne) [Internet]. 2012 Apr 25 [cited 2019 May 29];3:59. Available from: http://journal.frontiersin.org/article/10.3389/fendo.2012.00059/abstract

26. Vo BT, Khan SA. Expression of nodal and nodal receptors in prostate stem cells and prostate cancer cells: autocrine effects on cell proliferation and migration. Prostate [Internet]. 2011 Jul [cited 2019 May 29];71(10):1084–96. Available from: http://www.ncbi.nlm.nih.gov/pubmed/21557273

27. Strizzi L, Postovit L-M, Margaryan N V., Seftor EA, Abbott DE, Seftor REB, et al. Emerging Roles of Nodal and Cripto-1: From Embryogenesis to Breast Cancer Progression. Vonderhaar BK, Smith GH, editors. Breast Dis [Internet]. 2008 Oct 31 [cited 2019 May 25];29(1):91–103. Available from: http://www.medra.org/servlet/aliasResolver?alias=iospress&doi=10.3233/BD-2008-29110

28. Liu Y, Qin Z, Yang K, Liu R, Xu Y. Cripto-1 promotes epithelial-mesenchymal transition in prostate cancer via Wnt/β-catenin signaling. Oncol Rep [Internet]. 2017 Mar 1 [cited 2019 May 25];37(3):1521–8. Available from: https://www.spandidos-publications.com/10.3892/or.2017.5378

29. Wu Z, Li G, Wu L, Weng D, Li X, Yao K. Cripto-1 overexpression is involved in the tumorigenesis of nasopharyngeal carcinoma. BMC Cancer [Internet]. 2009 Dec 6 [cited 2019 May 25];9(1):315. Available from: http://bmccancer.biomedcentral.com/articles/10.1186/1471-2407-9-315

30. Boettcher M, McManus MT. Choosing the Right Tool for the Job: RNAi, TALEN, or CRISPR. Mol Cell [Internet]. 2015 May 21 [cited 2019 May 25];58(4):575–85. Available from: https://www.sciencedirect.com/science/article/pii/S109727651500310X

31. LaFountaine JS, Fathe K, Smyth HDC. Delivery and therapeutic applications of gene editing technologies ZFNs, TALENs, and CRISPR/Cas9. Int J Pharm [Internet]. 2015 Oct 15 [cited 2019 May 25];494(1):180–94. Available from: https://www.sciencedirect.com/science/article/pii/S0378517315301265

32. Gupta RM, Musunuru K. Expanding the genetic editing tool kit: ZFNs, TALENs, and CRISPR-Cas9. J Clin Invest [Internet]. 2014 Oct 1 [cited 2019 May 25];124(10):4154–61. Available from: https://www.jci.org/articles/view/72992

33. Doudna JA, Charpentier E. The new frontier of genome engineering with CRISPR-Cas9. Science (80-) [Internet]. 2014 Nov 28;346(6213):1258096–1258096. Available from: http://www.sciencemag.org/cgi/doi/10.1126/science.1258096

34. Sun CL, Barrangou R, Thomas BC, Horvath P, Fremaux C, Banfield JF. Phage mutations in response to CRISPR diversification in a bacterial population. Environ Microbiol [Internet]. 2013 Feb 1 [cited 2019 May 25];15(2):463–70. Available from: http://doi.wiley.com/10.1111/j.1462-2920.2012.02879.x

35. Hsu PD, Lander ES, Zhang F. Development and Applications of CRISPR-Cas9 for Genome Engineering. Cell [Internet]. 2014 Jun 5 [cited 2019 May 25];157(6):1262–78. Available from: https://www.sciencedirect.com/science/article/pii/S0092867414006047

36. Semenova E, Jore MM, Datsenko KA, Semenova A, Westra ER, Wanner B, et al. Interference by clustered regularly interspaced short palindromic repeat (CRISPR) RNA is governed by a seed sequence. Proc Natl Acad Sci [Internet]. 2011 Jun 21;108(25):10098–103. Available from: http://www.pnas.org/cgi/doi/10.1073/pnas.1104144108

37. Ran FA, Hsu PD, Lin C-Y, Gootenberg JS, Konermann S, Trevino AE, et al. Double Nicking by RNA-Guided CRISPR Cas9 for Enhanced Genome Editing Specificity. Cell [Internet]. 2013 Sep 12 [cited 2019 May 25];154(6):1380–9. Available from: https://www.sciencedirect.com/science/article/pii/S0092867413010155

38. CRISPR/Cas9 & Targeted Genome Editing: New Era in Molecular Biology [Internet]. [cited 2019 May 30]. Available from: https://international.neb.com/tools-and-resources/feature-articles/crispr-cas9-and-targeted-genome-editing-a-new-era-in-molecular-biology%0D

39. Marraffini LA, Sontheimer EJ. CRISPR interference limits horizontal gene transfer in staphylococci by targeting DNA. Science [Internet]. 2008 Dec 19 [cited 2019 May 25];322(5909):1843–5. Available from: http://www.ncbi.nlm.nih.gov/pubmed/19095942

40. Deltcheva E, Chylinski K, Sharma CM, Gonzales K, Chao Y, Pirzada ZA, et al. CRISPR RNA maturation by trans-encoded small RNA and host factor RNase III. Nature [Internet]. 2011 Mar 31 [cited 2019 May 25];471(7340):602–7. Available from: http://www.nature.com/articles/nature09886

41. Jinek M, Chylinski K, Fonfara I, Hauer M, Doudna JA, Charpentier E. A programmable dual RNA-guided DNA endonuclease in adaptive bacterial immunity. Science [Internet]. 2012 Aug 17 [cited 2019 May 30];337(6096):816. Available from: http://www.ncbi.nlm.nih.gov/pubmed/22745249

42. Chialva C, Eichler E, Muñoz C, Lijavetzky D. Development and Use of Biotechnology Tools for Grape Functional Analysis. In: Grape and Wine Biotechnology [Internet]. InTech; 2016 [cited 2019 May 25]. Available from: http://www.intechopen.com/books/grape-and-wine-

biotechnology/development-and-use-of-biotechnology-tools-for-grape-functional-analysis

43. Ranganathan V, Wahlin K, Maruotti J, Zack DJ. Expansion of the CRISPR-Cas9 genome targeting space through the use of H1 promoter-expressed guide RNAs. Nat Commun [Internet]. 2014 Aug 8 [cited 2019 May 30];5:4516. Available from: http://www.ncbi.nlm.nih.gov/pubmed/25105359

44. Haeussler M, Schönig K, Eckert H, Eschstruth A, Mianné J, Renaud J-B, et al. Evaluation of off-target and on-target scoring algorithms and integration into the guide RNA selection tool CRISPOR. Genome Biol [Internet]. 2016 Dec 5 [cited 2019 May 31];17(1):148. Available from: http://genomebiology.biomedcentral.com/articles/10.1186/s13059-016-1012-2

45. CrispOr [Internet]. Available from: http://crispor.tefor.net/

46. Ye J, Coulouris G, Zaretskaya I, Cutcutache I, Rozen S, Madden TL. Primer-BLAST: a tool to design target-specific primers for polymerase chain reaction. BMC Bioinformatics [Internet]. 2012 Jun 18 [cited 2019 May 31];13:134. Available from: http://www.ncbi.nlm.nih.gov/pubmed/22708584

47. Zuckerman JE, Hsueh T, Koya RC, Davis ME, Ribas A. siRNA Knockdown of Ribonucleotide Reductase Inhibits Melanoma Cell Line Proliferation Alone or Synergistically with Temozolomide. J Invest Dermatol [Internet]. 2011 Feb 1 [cited 2019 May 27];131(2):453–60. Available from: https://www.sciencedirect.com/science/article/pii/S0022202X15351599

48. Gaj T, Gersbach CA, Barbas CF. ZFN, TALEN, and CRISPR/Cas-based methods for genome engineering. Trends Biotechnol [Internet]. 2013 Jul;31(7):397–405. Available from: https://linkinghub.elsevier.com/retrieve/pii/S0167779913000875

49. Stepanenko AA, Heng HH. Transient and stable vector transfection: Pitfalls, off-target effects, artifacts. Mutat Res Mutat Res [Internet]. 2017 Jul 1 [cited 2019 May 25];773:91–103. Available from: https://www.sciencedirect.com/science/article/pii/S1383574216300357

50. Glass Z, Lee M, Li Y, Xu Q. Engineering the Delivery System for CRISPR-Based Genome Editing. Trends Biotechnol [Internet]. 2018 Feb 1 [cited 2019 May 25];36(2):173–85. Available from: https://www.sciencedirect.com/science/article/pii/S0167779917303049

51. Lino CA, Harper JC, Carney JP, Timlin JA. Delivering CRISPR: a review of the challenges and approaches. Drug Deliv [Internet]. 2018 Jan 25 [cited 2019 Apr 27];25(1):1234–57. Available from: https://www.tandfonline.com/doi/full/10.1080/10717544.2018.1474964

52. Liang X, Potter J, Kumar S, Zou Y, Quintanilla R, Sridharan M, et al. Rapid and highly efficient mammalian cell engineering via Cas9 protein transfection. J Biotechnol [Internet]. 2015 Aug 20 [cited 2019 May 25];208:44–53. Available from: https://www.sciencedirect.com/science/article/pii/S016816561500200X

53. Fu Y, Foden JA, Khayter C, Maeder ML, Reyon D, Joung JK, et al. High-frequency off-target mutagenesis induced by CRISPR-Cas nucleases in human cells. Nat Biotechnol [Internet]. 2013 Sep 23 [cited 2019 May 25];31(9):822–6. Available from: http://www.nature.com/articles/nbt.2623

54. Kim S, Kim D, Cho SW, Kim J, Kim J-S. Highly efficient RNA-guided genome editing in human cells via delivery of purified Cas9 ribonucleoproteins. Genome Res [Internet]. 2014

Jun [cited 2019 May 31];24(6):1012–9. Available from: http://www.ncbi.nlm.nih.gov/pubmed/24696461

55. Zuris JA, Thompson DB, Shu Y, Guilinger JP, Bessen JL, Hu JH, et al. Cationic lipid-mediated delivery of proteins enables efficient protein-based genome editing in vitro and in vivo. Nat Biotechnol [Internet]. 2015 Jan 30 [cited 2019 May 31];33(1):73–80. Available from: http://www.nature.com/articles/nbt.3081

56. Khan AA, El-Sayed A, Akbar A, Mangravita-Novo A, Bibi S, Afzal Z, et al. A highly efficient ligation-independent cloning system for CRISPR/Cas9 based genome editing in plants. Plant Methods [Internet]. 2017 Dec 16 [cited 2019 May 25];13(1):86. Available from: http://plantmethods.biomedcentral.com/articles/10.1186/s13007-017-0236-9

57. Shuman S. Novel approach to molecular cloning and polynucleotide synthesis using vaccinia DNA topoisomerase. J Biol Chem [Internet]. 1994 Dec 23 [cited 2019 May 31];269(51):32678–84. Available from: http://www.ncbi.nlm.nih.gov/pubmed/7798275

58. Udo H. An Alternative Method to Facilitate cDNA Cloning for Expression Studies in Mammalian Cells by Introducing Positive Blue White Selection in Vaccinia Topoisomerase I-Mediated Recombination. PLoS One [Internet]. 2015 [cited 2019 May 31];10(9):e0139349. Available from: http://www.ncbi.nlm.nih.gov/pubmed/26422141

59. Kreiss P, Mailhe P, Scherman D, Pitard B, Cameron B, Rangara R, et al. Plasmid DNA size does not affect the physicochemical properties of lipoplexes but modulates gene transfer efficiency. Nucleic Acids Res [Internet]. 1999 Oct 1 [cited 2019 May 25];27(19):3792–8. Available from: https://academic.oup.com/nar/article-lookup/doi/10.1093/nar/27.19.3792

60. Burkhart A, Andresen TL, Aigner A, Thomsen LB, Moos T. Transfection of primary brain capillary endothelial cells for protein synthesis and secretion of recombinant erythropoietin: a strategy to enable protein delivery to the brain. Cell Mol Life Sci [Internet]. 2017 Jul 14 [cited 2019 May 25];74(13):2467–85. Available from: http://link.springer.com/10.1007/s00018-017-2501-5

61. Thomas P, Smart TG. HEK293 cell line: A vehicle for the expression of recombinant proteins. J Pharmacol Toxicol Methods [Internet]. 2005 May 1 [cited 2019 May 27];51(3):187–200. Available from: https://www.sciencedirect.com/science/article/pii/S1056871905000110?via%3Dihub

62. Hagemann C, Meyer C, Stojic J, Eicker S, Gerngras S, Kühnel S, et al. High efficiency transfection of glioma cell lines and primary cells for overexpression and RNAi experiments. J Neurosci Methods [Internet]. 2006 Sep 30 [cited 2018 Nov 8];156(1–2):194–202. Available from: https://www.sciencedirect.com/science/article/pii/S0165027006001403?via%3Dihub

63. Jordan M, Wurm F. Transfection of adherent and suspended cells by calcium phosphate. Methods [Internet]. 2004 Jun 1 [cited 2019 May 31];33(2):136–43. Available from: https://www.sciencedirect.com/science/article/pii/S1046202303003050

64. Marucci G, Lammi C, Buccioni M, Dal Ben D, Lambertucci C, Amantini C, et al. Comparison and optimization of transient transfection methods at human astrocytoma cell line 1321N1. Anal Biochem [Internet]. 2011 Jul 15 [cited 2019 May 25];414(2):300–2. Available from: https://www.sciencedirect.com/science/article/pii/S000326971100131X

65. Zerrouqi A, Rixe O, Ghoumari AM, Yarovoi S V, Mouawad R, Khayat D, et al. Liposomal

delivery of the herpes simplex virus thymidine kinase gene in glioma: improvement of cell sensitization to ganciclovir. Cancer Gene Ther [Internet]. 1996 [cited 2019 May 25];3(6):385–92. Available from: http://www.ncbi.nlm.nih.gov/pubmed/8988841

66. Distler JHW, Jungel A, Kurowska-Stolarska M, Michel BA, Gay RE, Gay S, et al. Nucleofection: a new, highly efficient transfection method for primary human keratinocytes*. Exp Dermatol [Internet]. 2005 Apr 1 [cited 2019 May 25];14(4):315–20. Available from: http://doi.wiley.com/10.1111/j.0906-6705.2005.00276.x

67. Potter H, Heller R. Transfection by Electroporation. Curr Protoc Mol Biol [Internet]. 2003 May [cited 2019 May 25];CHAPTER:Unit. Available from: http://www.ncbi.nlm.nih.gov/pubmed/18265334

68. Pilgaard L, Mortensen JH, Henriksen M, Olesen P, Sørensen P, Laursen R, et al. Cripto-1 expression in glioblastoma multiforme. Brain Pathol [Internet]. 2014 Jul [cited 2018 Sep 27];24(4):360–70. Available from: http://www.ncbi.nlm.nih.gov/pubmed/24521322

69. Tysnes BB, Satran HA, Mork SJ, Margaryan N V, Eide GE, Petersen K, et al. Age-Dependent Association between Protein Expression of the Embryonic Stem Cell Marker Cripto-1 and Survival of Glioblastoma Patients. Transl Oncol [Internet]. 2013 Dec 1 [cited 2018 Oct 9];6(6):732–41. Available from: http://www.ncbi.nlm.nih.gov/pubmed/24466376

70. Alowaidi F, Hashimi SM, Nguyen M, Meshram M, Alqurashi N, Cavanagh BL, et al. Investigating the role of CRIPTO-1 (TDGF-1) in glioblastoma multiforme U87 cell line. J Cell Biochem [Internet]. 2018 Nov 13 [cited 2018 Nov 18]; Available from: http://doi.wiley.com/10.1002/jcb.28015

71. Alowaidi F, Hashimi SM, Nguyen M, Meshram M, Alqurashi N, Cavanagh BL, et al. Investigating the role of CRIPTO-1 (TDGF-1) in glioblastoma multiforme U87 cell line. J Cell Biochem [Internet]. 2019 May 13 [cited 2018 Dec 31];120(5):7412–27. Available from: http://doi.wiley.com/10.1002/jcb.28015

72. Gudbergsson JM, Kostrikov S, Johnsen KB, Fliedner FP, Stolberg CB, Humle N, et al. A tumorsphere model of glioblastoma multiforme with intratumoral heterogeneity for quantitative analysis of cellular migration and drug response. Exp Cell Res [Internet]. 2019 Jun 1 [cited 2019 May 27];379(1):73–82. Available from: https://www-sciencedirect-com.zorac.aub.aau.dk/science/article/pii/S0014482719301314

7. Appendix

Lipofectamine transfection	Transfection efficiency (eGFP %)	Live/dead assay (PI %)
First Hek293T transfection **3/9**	SpL – 11.17, 10.47, 10 SpM – 10.46, 7.38, 9.6 SpH – 4.19, 2.4, 5.17 Ev – 0.67 Average: 7.871	SpL – 3.82, 4.51, 3.34 SpM – 4.39, 3.45, 3.91 SpH – 5.33, 1.83, 4.83 NTC – 3.25, 4, 4 Ev – 3.64
Second Hek293T transfection (48 hours post transfection) **13/09**	SpL – 18.25, 18.25, 18.53 SpH – 15.79, 16.69, 15.86 Ev – 0.33, 0.33 Average: 17.22	SpL – 4.44, 5.6, 4.83 SpH -5.19, 7.13, 5 Ev – 4.83, 4.26 Pl – 4.28, 4.2 NTC – 3.23, 5.49, 4.42, 4.36
Second Hek293T transfection (72 hours post transfection) **14/09**	SpL – 13.35, 15.43 SpH – 12.72, 14.37 Ev- 0,53 Average: 13.96	SpL – 0.8, 0.13 SpH –0.36, 0.13 Ev – 2.77 NTC – 4.7, 5.79, 6.85
First U87 transfection DLJ 25/10	Spl -0, 0, 0 % Sph 0, 0, 0 % Average: 0	Spl – 1.4, 1.88, 2.59 Sph – 2.48, 2.8, 1.7 NTC – 2.6, 2.77, 2.69
Second U-87 transfection SplM 31/10	SplM - 2.67, 2.8, 2.18, 3.21 Average: 2.715	SplM – 4, 5.4, 9 NTC – 1.71, 1.9, 2.29, 2.32
Third U87 Transfection DLJ 10/11	SpL – 13.33, 1.58, 12,98 SpM – 1,44, 0,81, 0,38 Average: 5.16	SpL – 1.17, 0.63 SpM – 0.2, 0.69 NTC – 0.64, 0.76, 0.79, 1.67 Ev – 0.53
Fourth U87 Transfection DLJ 15/11	SpM -12.81, 14, 13.71, 10.52 EpO – 21.59, 22.37, 23.29 Average: 12.7 (of spcas9)	SpM – 2.19, 4.16, 3.2, EpO – 2.68 NTC – 2.97, 2.62
Fifth U87 Transfection DLJ 21/11	SpM -5.44, 3.62, 4.51 SpL – 3.44, 2.36, 3.44 Average: 3.8	ND*
First Ntera2 Transfektion DLJ 07/02	Spm- 5.85, 3.8, 4.55, 5.78 Sph- 5.39, 10.34, 10, 7 Average: 6.59	ND*

Supplementary Table 1: Transfection efficiencies and cell viability measurements 48 hours (and for one 72 hours) after each Lipofectamine optimization. ND- not determined Sp- Spcas9(PX461), L – low, M- Medium, H- High (Low, medium or high amount of DNA or Lipofectamine (different for each optimization)). Epo- a smaller plasmid than Spcas9(PX461) used to assess whether plasmid size affected efficiency. NTC- non-transfected. Ev- emptyvector control. Pl – plasmid control (no DNA only lipofectamine)

Calcium phosphate transfection	Transfection efficiency (eGFP %)
Cell: U87 Date: 16/11	SpM – 3.6, 0.5, 1.24, 2.51 Sph – 0.59, 0.29, 0.3, 0.21 Average: 1.15
Cell: U87 Date: 28/3	SL – 8.52, 12.39, 13.9, 16.17, 19.5, 17.24 SH – 15.47, 16.5, 12.68, 11.25, 15.52 Average: 14.46

Supplementary Table 2: Transfection efficiency of Two calcium phosphate setups. Sp- Spcas9(PX461), L – low, M- Medium, H- High (Low, medium or high amount of DNA (different for each optimization)).

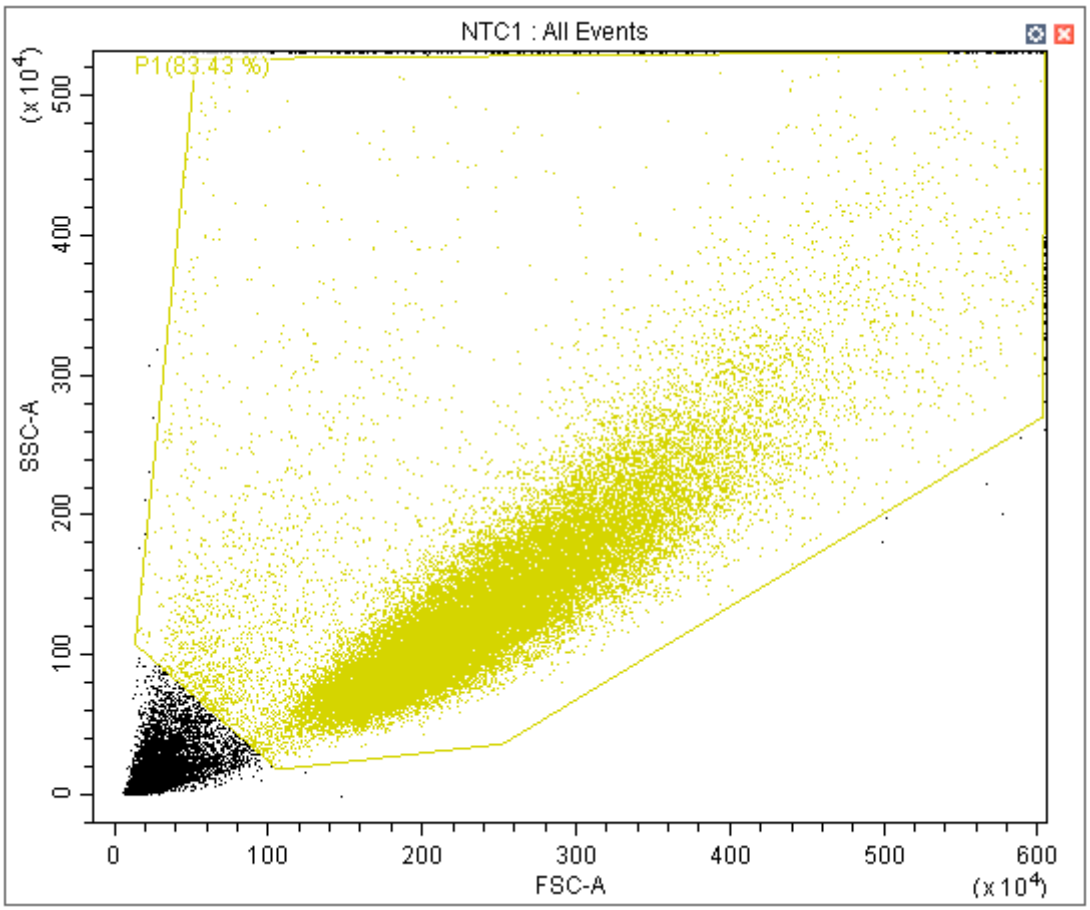

Supplementary Figure 1: When analyzing the transfections mentioned in Supplementary table 1 and 2 on a flow cytometer gating of cells was performed in a FCS-A/SSC-A-plot.

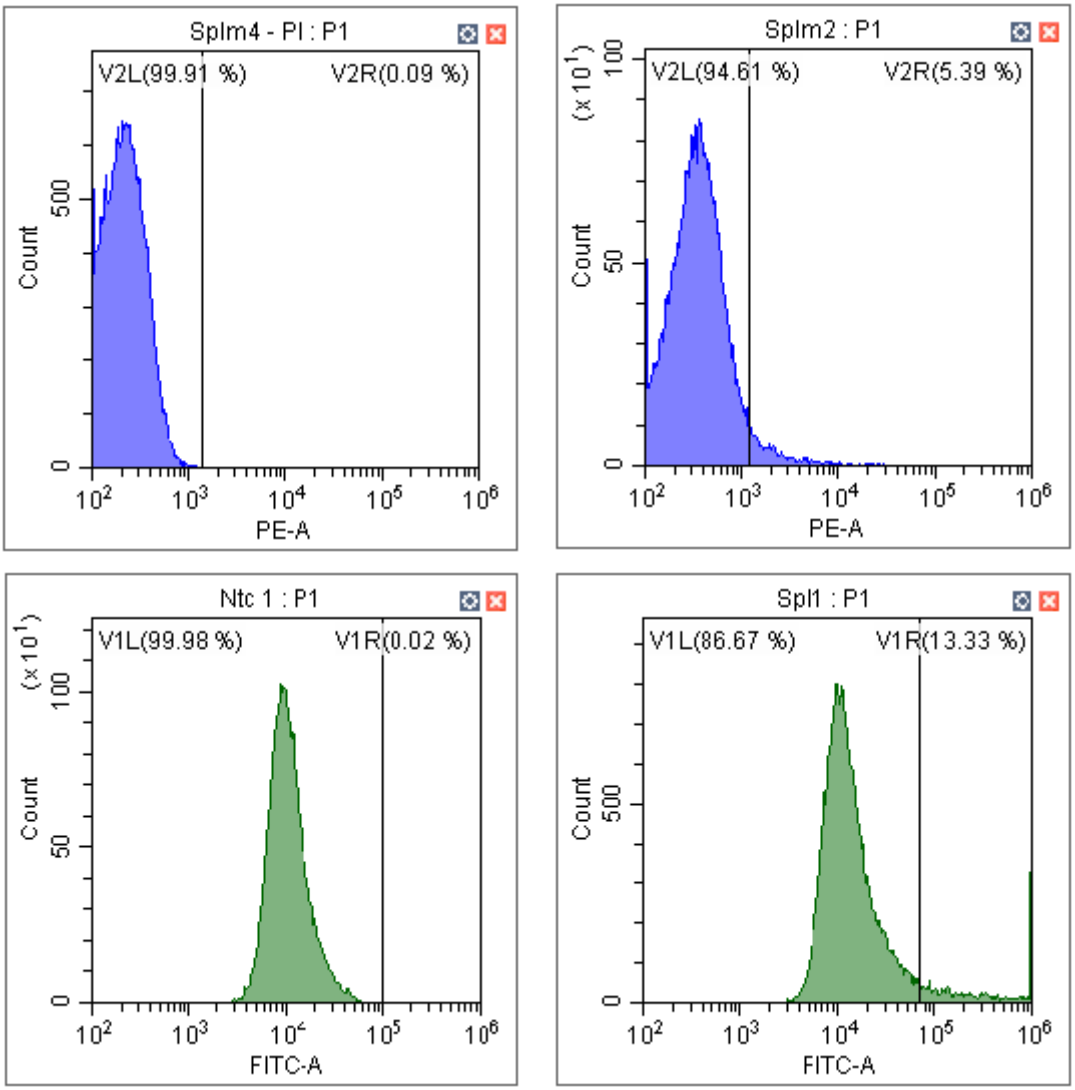

Supplementary Figure 2: eGFP from events was measured in the FITC-Area channel. To identify eGFP-signaling in transfected samples a Vertical border was set in the FITC-A channel using NTC-samples. To measure viability of transfected cells, Propidium Iodide(PI) was added before analyzing on the flow-cytometer. Propidium Iodide is measured in the PE-Area gate, and samples with no addition of PI was used to set the vertical border discriminating signaling from PI.

2018 -12 -17

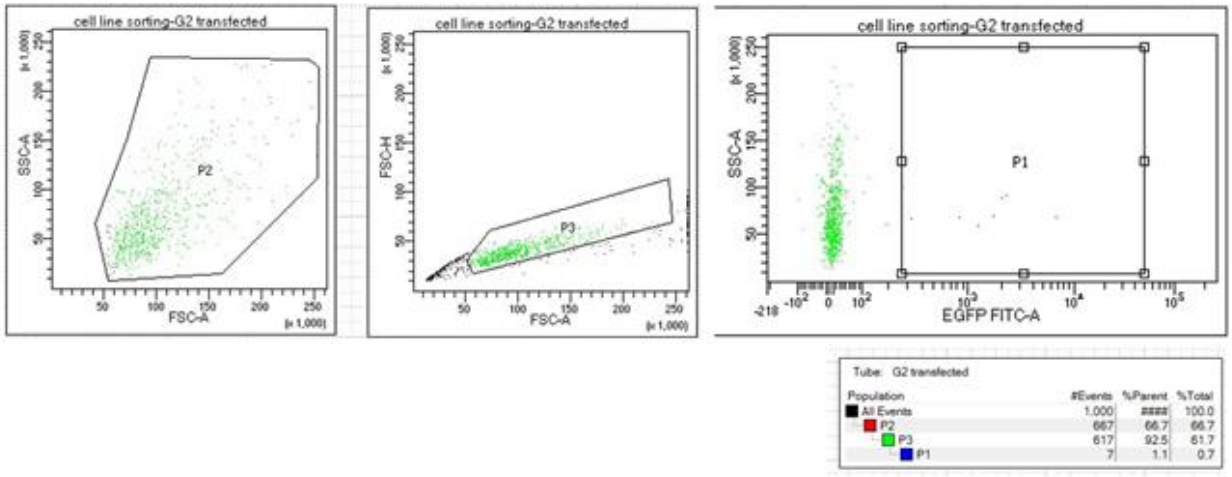

Name of transfected sample	Percentage eGFP+ (of gate)	Total cells sorted
sgRNA2	0.1-0.5%	1800 cells
sgRNA3	0.5-1.3 %	1900 cells
sgRNA4	0.2-0.3%	700 cells

Supplementary Figure/Table 3: The 15/12 2018 U87 cells were transfected with sgRNA2,3 and 4 using lipofectamine. Unfortunately, as can be seen in the P1 gate of sgRNA4 transfected cells above, very few cells were expressing eGFP. Of all gated events less than 1,4 % of all cells were eGFP-producing. Due to this low transfection efficiency less than 2000 cells were sorted from sgRNA2 and 3 transfected cells. For sgRNA4 only 700 cells could be isolated based signaling in the FITC-A gate. The transfection efficiency was thus lower than several of the optimized lipofectamine transfections on U87 performed prior to this (see supplementary Table 1).

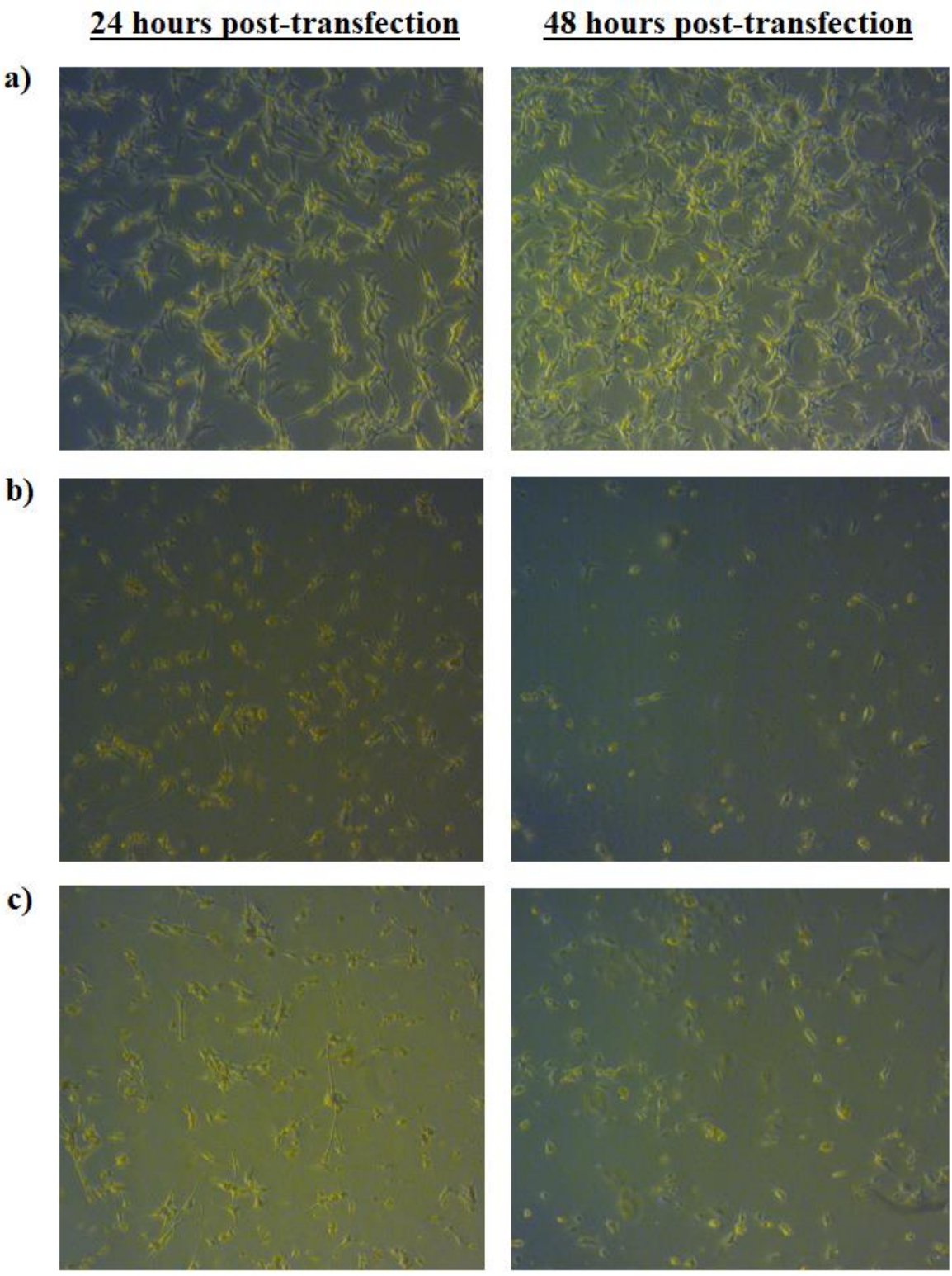

Supplementary Figure 4: 24 and 48 hours after Calcium phosphate transfection of U87 the 2/4 2019 (methods section 2.11) microscopy photos was taken on a Zeiss Primovert microscope at 10X magnification. As observed the non-transfected control (a) became more confluent as time passed, while the samples transfected with Non-target (b) and sgRNA1(c) cloned plasmids became less confluent.

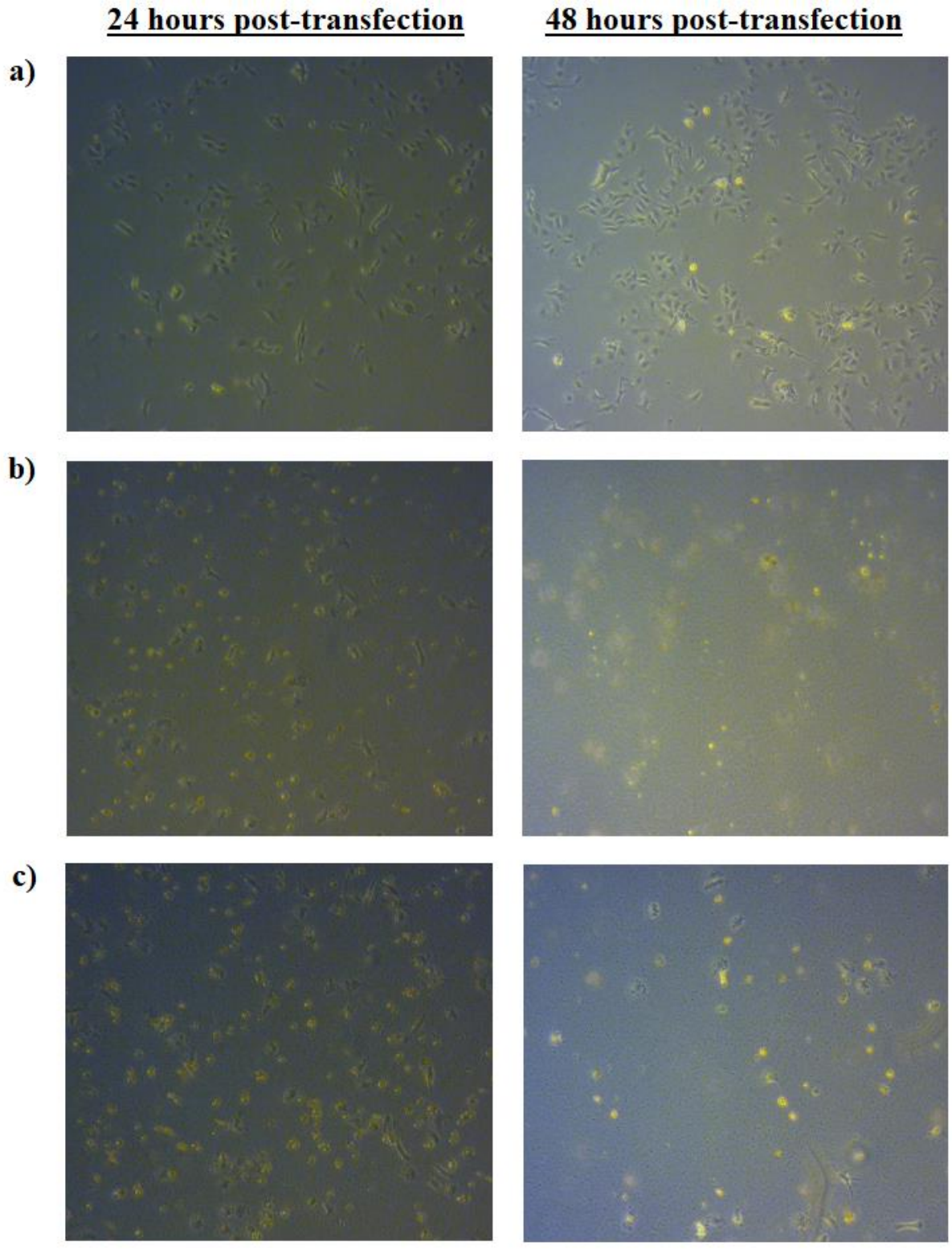

Supplementary Figure 5: 24 and 48 hours after Calcium phosphate transfection of Ntera2 the 2/4 2019 (methods section 2.11), the NTCs(a) became more confluent during the 48 hours after transfection, while while the samples transfected with Non-target (b) and sgRNA1(c) cloned plasmids became less confluent.

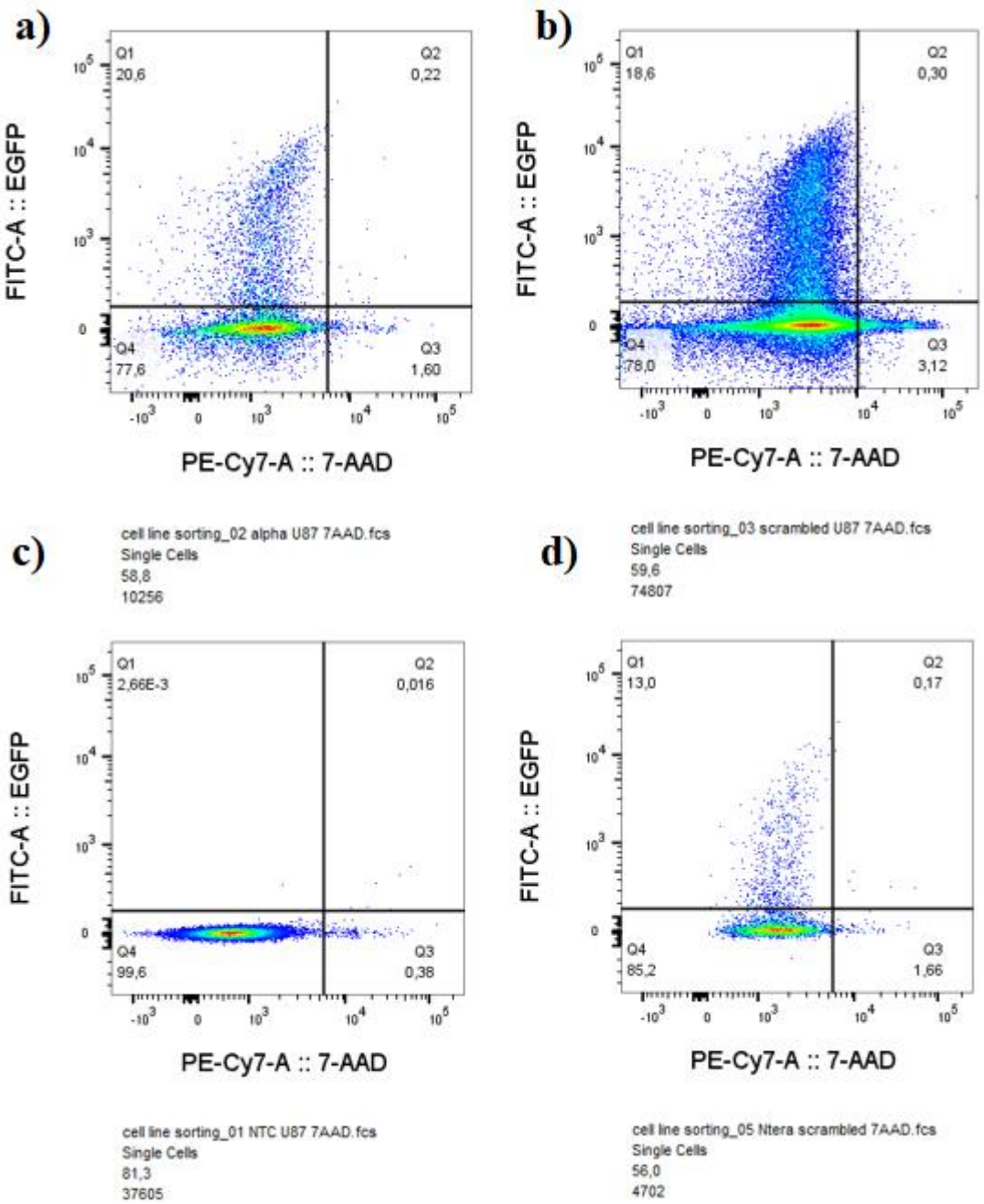

Supplementary Figure 6: The Calcium phosphate transfection performed 2/4 2019 produced efficiencies of 20,6 % (Q1) in the U87 cells transfected with sgRNA1 cloned plasmids (a) which were higher than the previous Calcium phosphate transfections (Supplementary table 2). The efficiency were 18,6 % (Q1) for U87 transfected with Non-target RNA (b). Most gated cells were alive since the eGFP+ (Q2) and eGFP-(Q3) fraction positive for 7-AAD were very low (less than 4 % in the sample with the highest amount of 7-AAD+ events). NTC(c) was used to set the vertical border dividing eGFP+ from eGFP-. Flowsorting of Ntera2(d) samples was not completed since too few events where recorded. This is not surprising since very few cells were present in the sgRNA1 and Non-target transfected Ntera2 when observed under a microscope (Supplementary Figure 5). For sgRNA1 transfected U87 a total of 24.500 cells were sorted, while for the Non-target transfected, 8.200 cells were sorted.

Supplementary Figure 7: Sequencing chromatogram with the location of the identified sgRNA1 marked with a red circle.

Supplementary Figure 8: Sequencing chromatogram with the identified sgRNA2 marked with a red circle

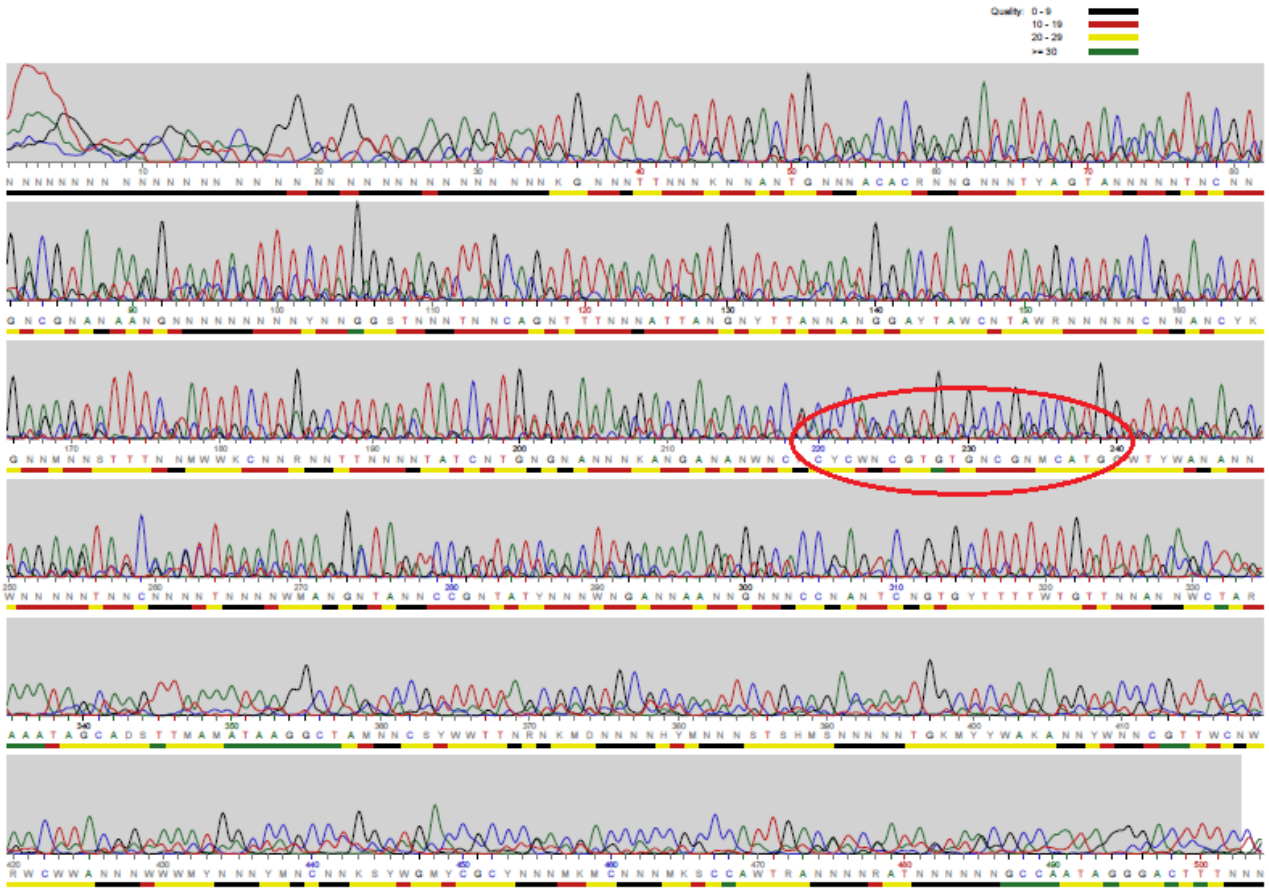

Supplementary Figure 9: Sequencing chromatogram with the identified sgRNA3 marked with a red circle. Despite lots of interference the sgRNA was easily located in the expected region (approximately sanger signal 220-240) when performing alignment (see results section 3.5).

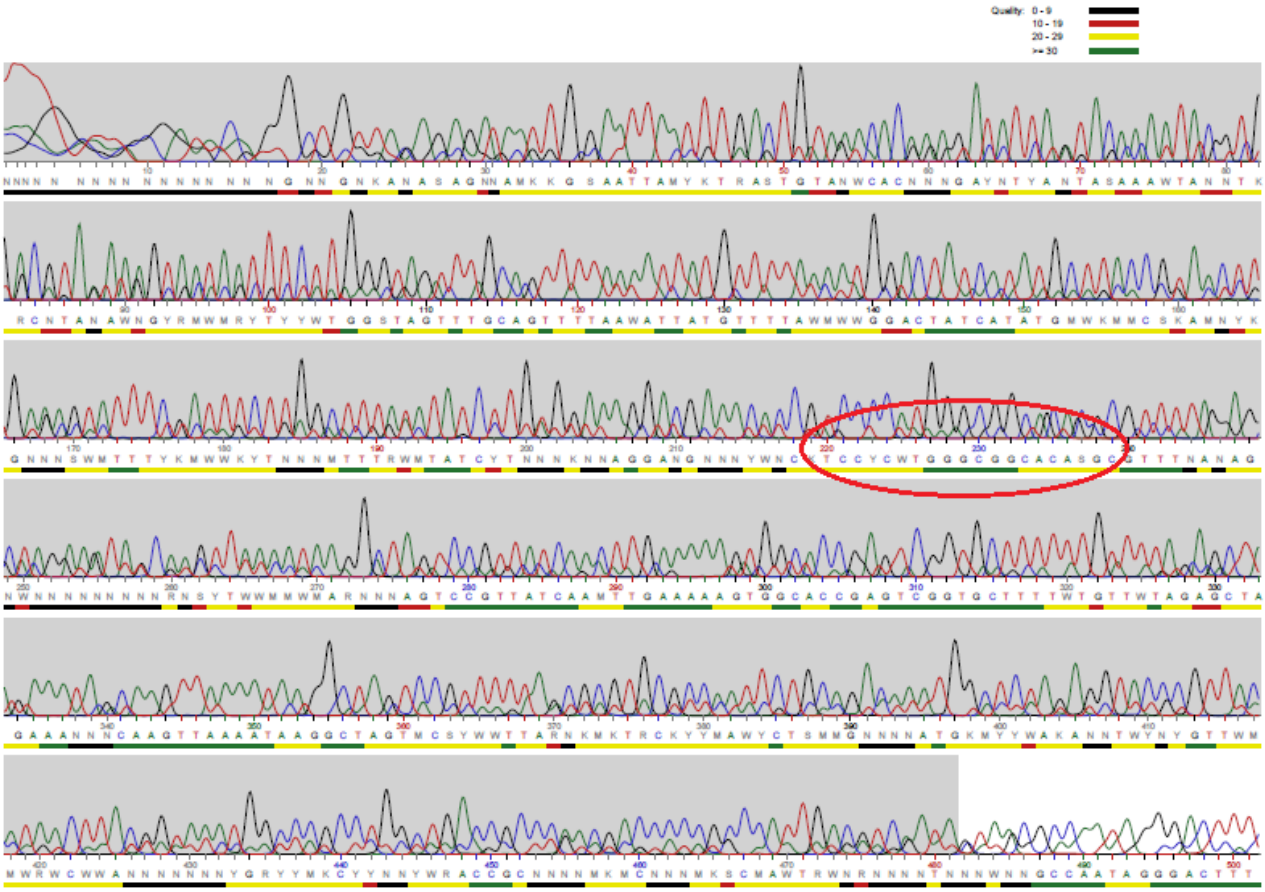

Supplementary Figure 10: Sequencing chromatogram with the identified sgRNA4 marked with a red circle. Despite lots of interference the sgRNA was easily located in the expected region (approximately sanger signal 220-240) when performing alignment (see results section 3.5).

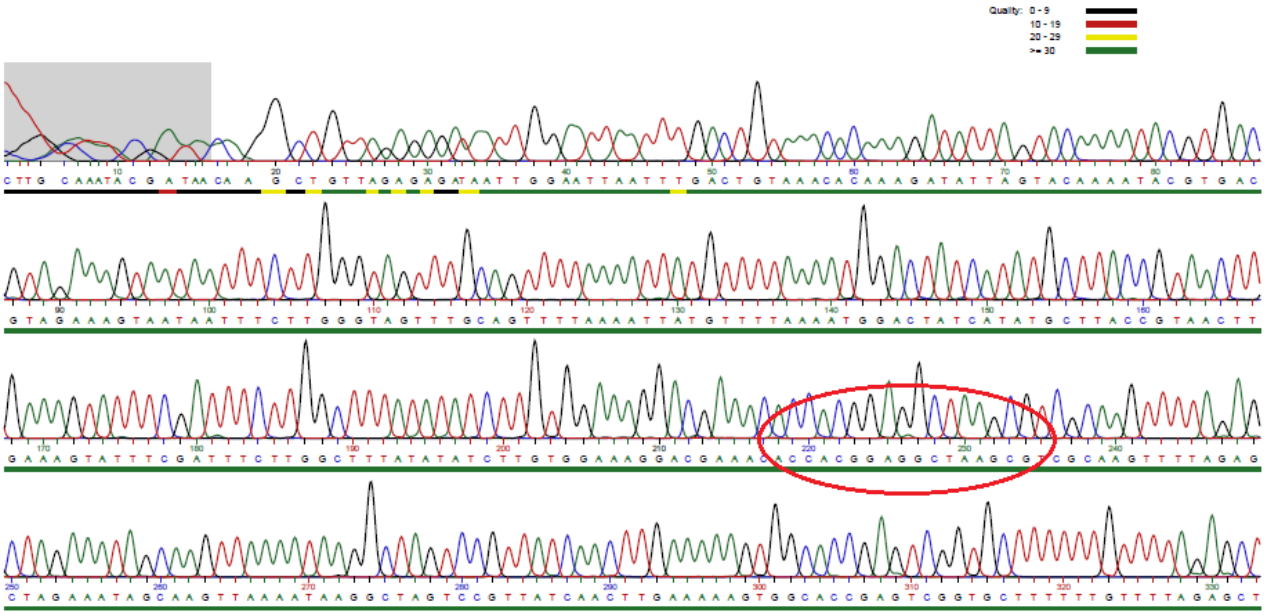

Supplementary Figure 11: Sequencing Chromatogram with identified Non-target RNA marked with a red circle.

Supplementary Figure 12: when receiving sequencing results from extracted plasmids (see methods section 2.10) alignment was performed between sanger output and the sequence normally present in the PX461 prior to BbsI-cleavage (5'CACCGGGTCTTCGAGAAGACCT3'), to assess whether it had been removed. The above example is alignment between the pre-cleavage sequence and the sgRNA1 output that turned out to be a successful cloning (results section 3.5). The alignment showed that the pre-cleavage sequence had been removed. The alignment between the ten bases at position 284-293 should not be viewed as a the pre-cleavage sequence since the 5'CACCGAGTCG3'-sequence is present 62 bps downstream of the cleavage site regardless of whether BbsI has cleaved or not.

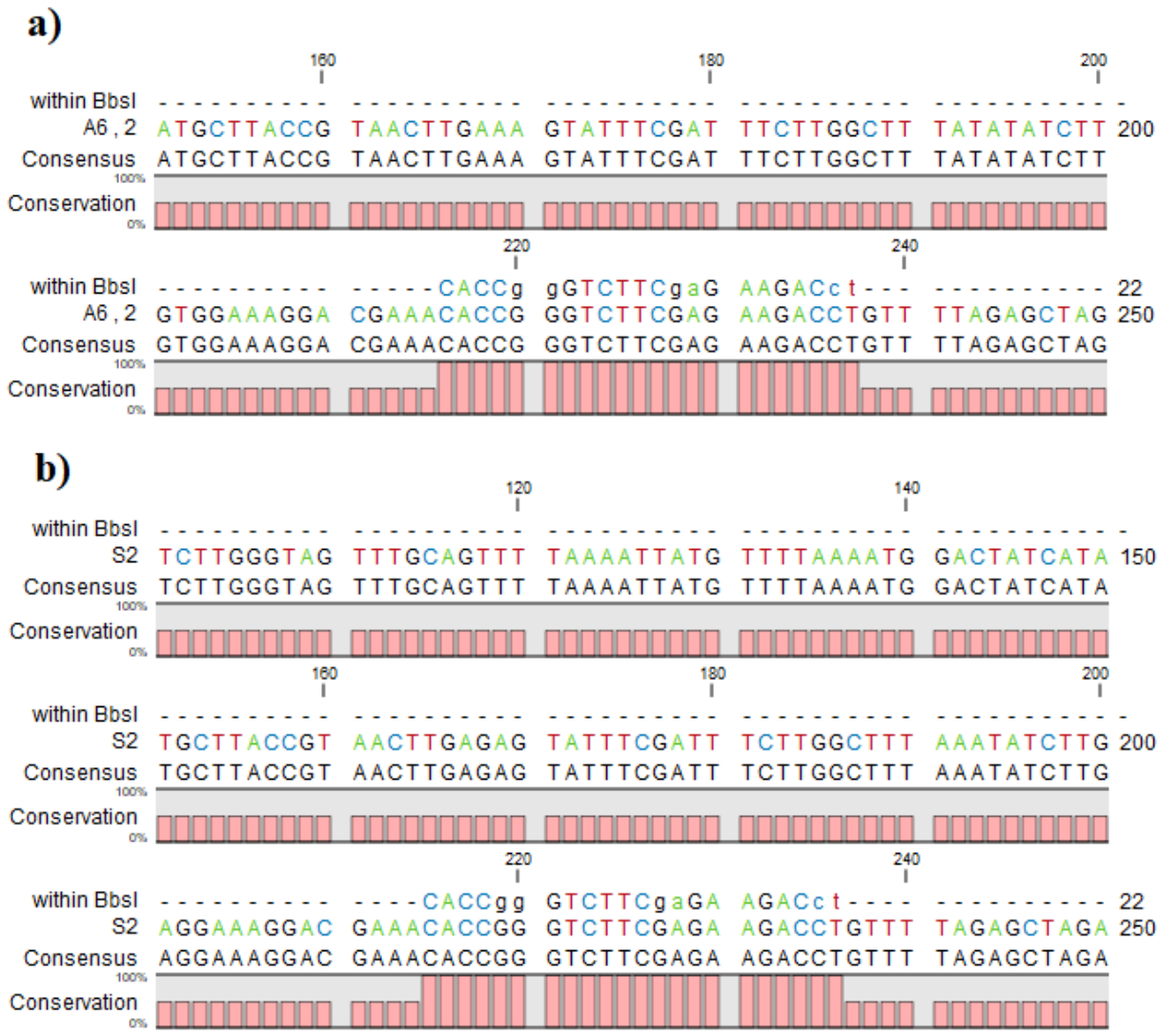

Supplementary Figure 13: two examples of failed cloning as alignment showed that the pre-cleavage sequence (5'CACCGGGTCTTCGAGAAGACCT3') was present in the sanger outputs, and BbsI-cleavage had thus not taken place in the attempted sgRNA1 (a) and Non-target RNA (b) cloned samples.

Amount cells	DNA conc.	260/280-ratio	260/230-ratio
$0.25*10^6$	20.9 ng/µl	1.92	1.45
$0.5*10^6$	51.3 ng/µl	1.94	1.9
$1*10^6$	142.2 ng/µl	1.915	2.19
$2*10^6$	234.8 ng/µl	2	2.145

Supplementary Table 4: DNA-concentrations, 260/280- and 260/230-ratios of extracted genomic DNA from 250.000, 500.000, 1 mio. and 2 mio. Hek293t cells. Based on the 260/230 ratio 1 mio. and 2 mio. cells appeared to be the best amount of cells to extract gDNA from, but 500.000 cells was also acceptable.

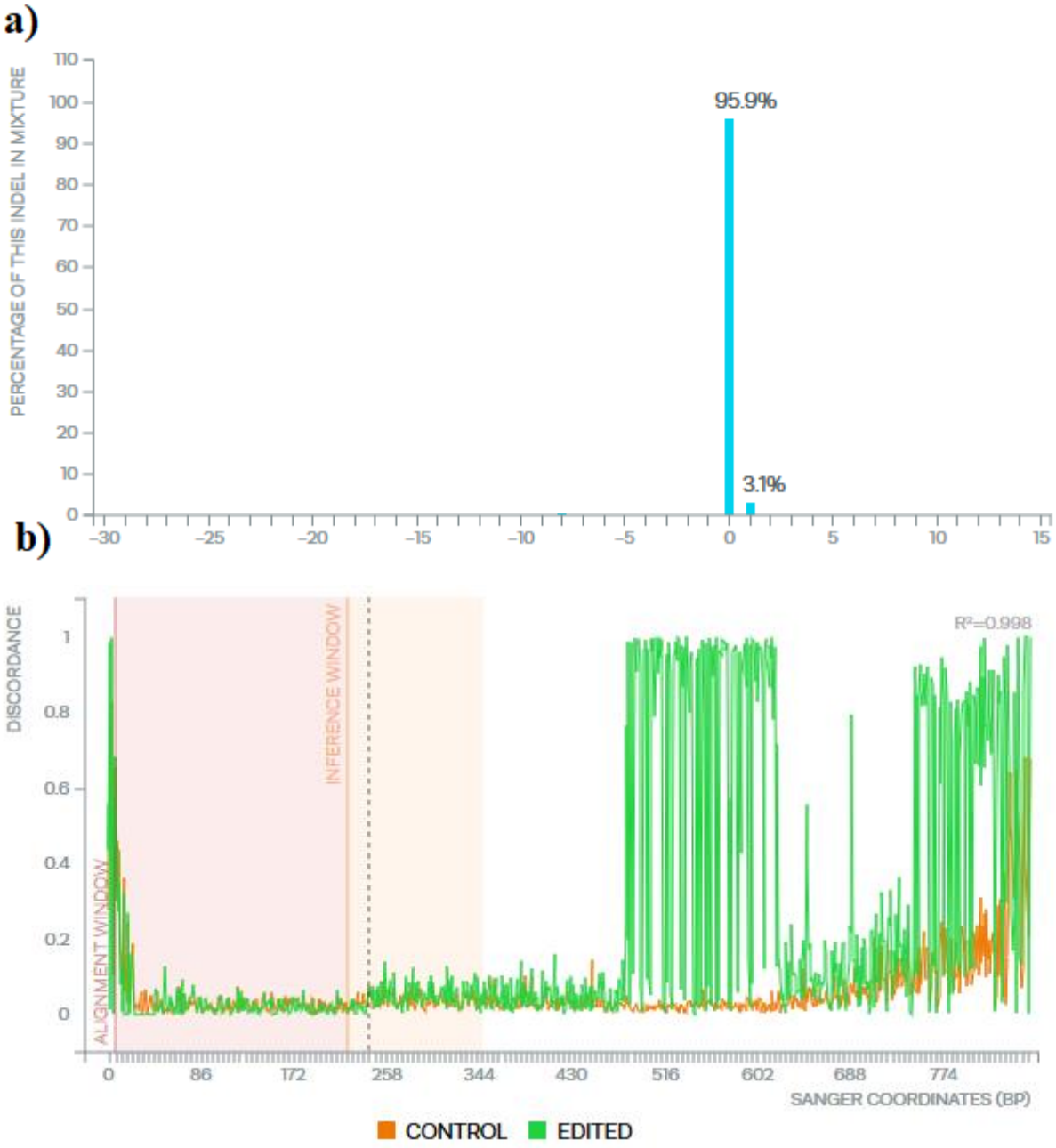

Supplementary Figure 14: Indel distributions with the Indel plot (a). The X-axis on the indel plot represents size of the deletion (on the left side of zero) or insertion (on the right side of zero). Zero represents no indels (or unedited). The Y-axis represents the percentage of the treated sample with a given Indel. The discordance plot (b) shows degree of signal-differences between the treated (edited) and untreated (control) for each base in the sanger-outputs. The alignment window is the region on the sanger output of the control and edited sample that were aligned. The interference window is the located cut-site region. The X-axis is the base pair position on the sequencing output, The Y-axis Is the level of discordance between the edited and control sample. If CRISPR-editing is successful we would expect a high level of discordance at and after the cut-site, but a low level of discordance before the cut-site.

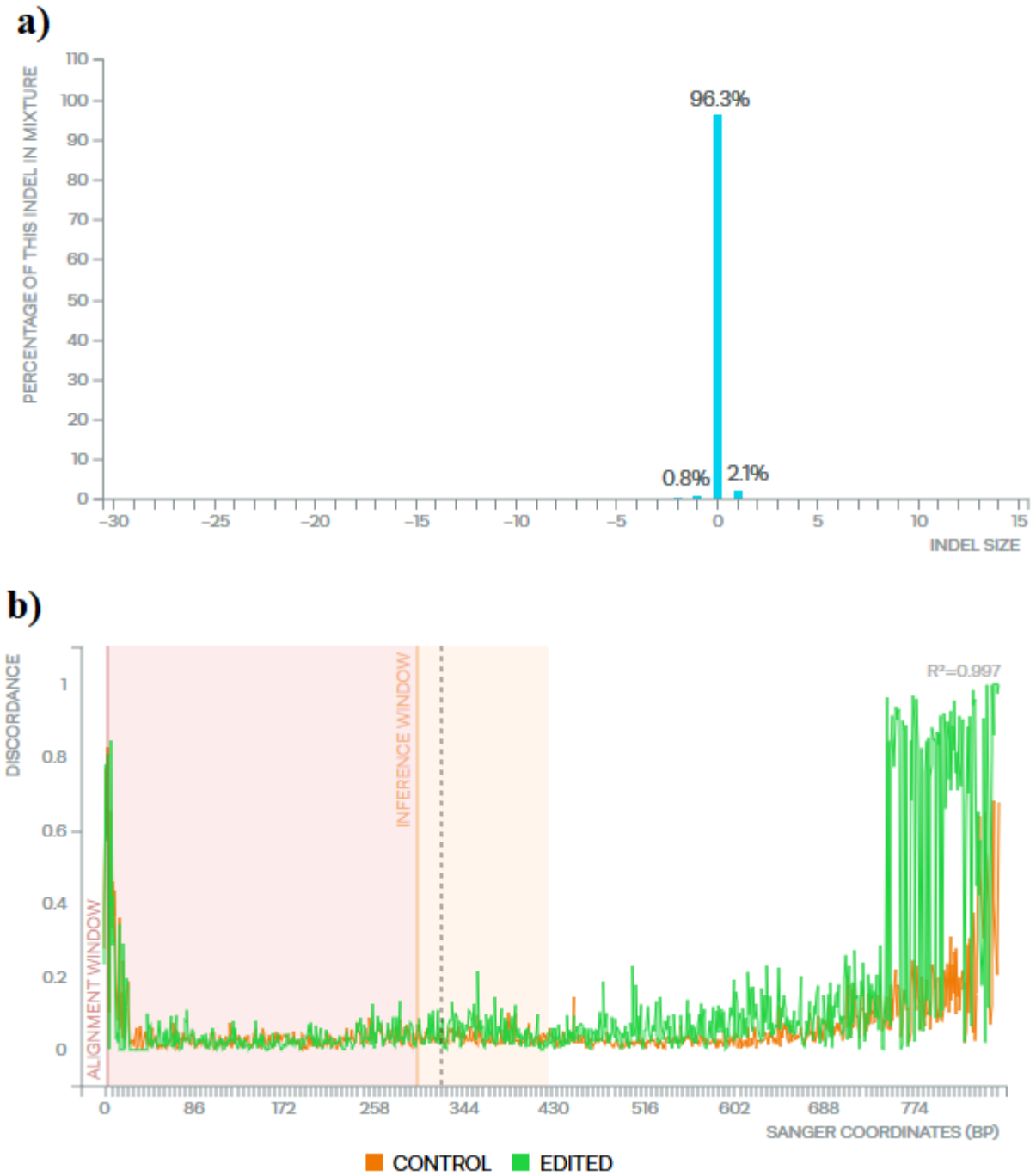

Supplementary Figure 15: Indel distributions with the Indel plot (a). The X-axis on the indel plot represents size of the deletion (on the left side of zero) or insertion (on the right side of zero). Zero represents no indels (or unedited). The Y-axis represents the percentage of the treated sample with a given Indel. The discordance plot (b) shows degree of signal-differences between the treated (edited) and untreated (control) for each base in the sanger-outputs. The alignment window is the region on the sanger output of the control and edited sample that were aligned. The interference window is the located cut-site region. The X-axis is the base pair position on the sequencing output, The Y-axis Is the level of discordance between the edited and control sample. If CRISPR-editing is successful we would expect a high level of discordance at and after the cut-site, but a low level of discordance before the cut-site.

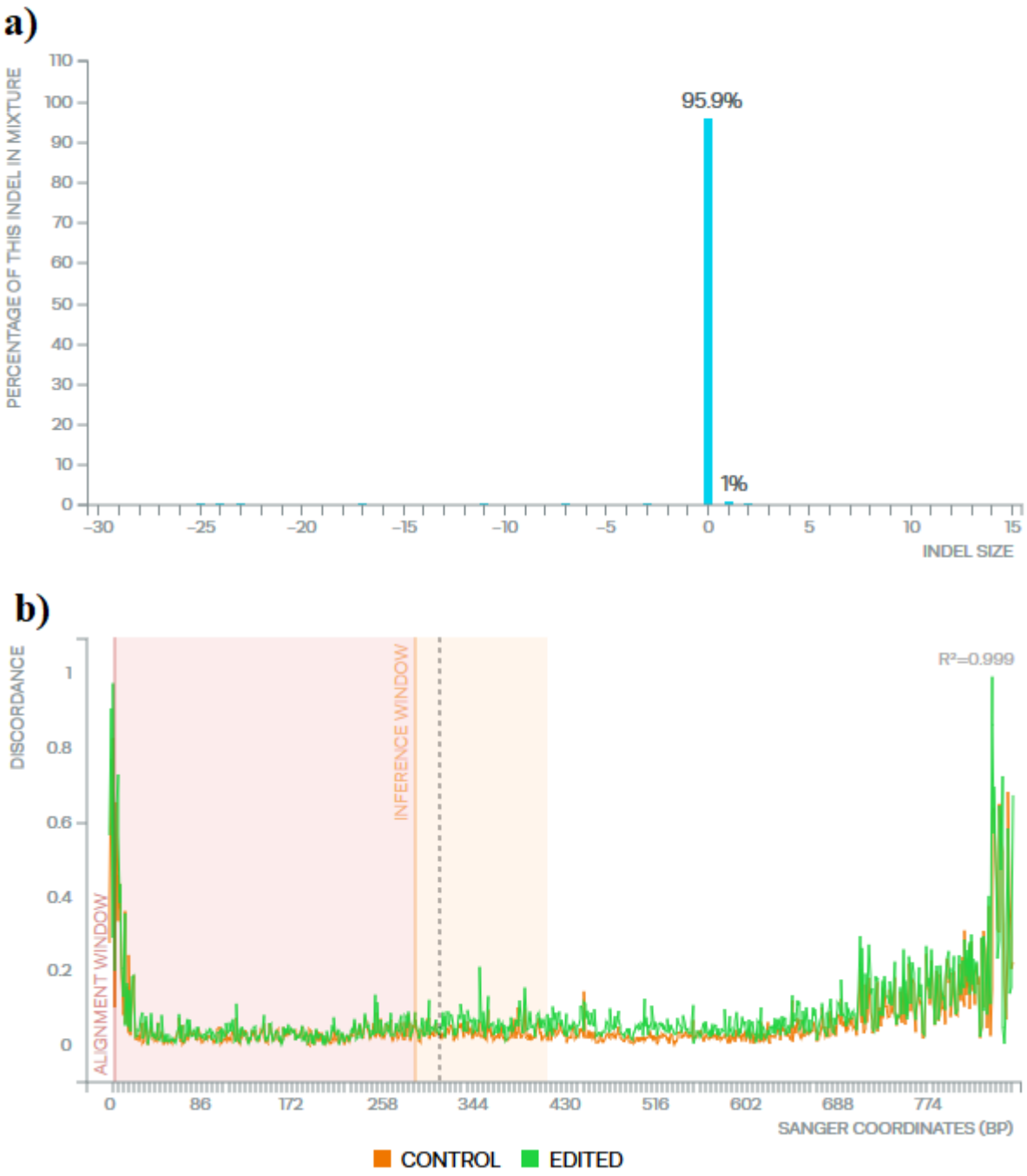

Supplementary Figure 16: Indel distributions with the Indel plot (a). The X-axis on the indel plot represents size of the deletion (on the left side of zero) or insertion (on the right side of zero). Zero represents no indels (or unedited). The Y-axis represents the percentage of the treated sample with a given Indel. The discordance plot (b) shows degree of signal-differences between the treated (edited) and untreated (control) for each base in the sanger-outputs. The alignment window is the region on the sanger output of the control and edited sample that were aligned. The interference window is the located cut-site region. The X-axis is the base pair position on the sequencing output, The Y-axis Is the level of discordance between the edited and control sample. If CRISPR-editing is successful we would expect a high level of discordance at and after the cut-site, but a low level of discordance before the cut-site.

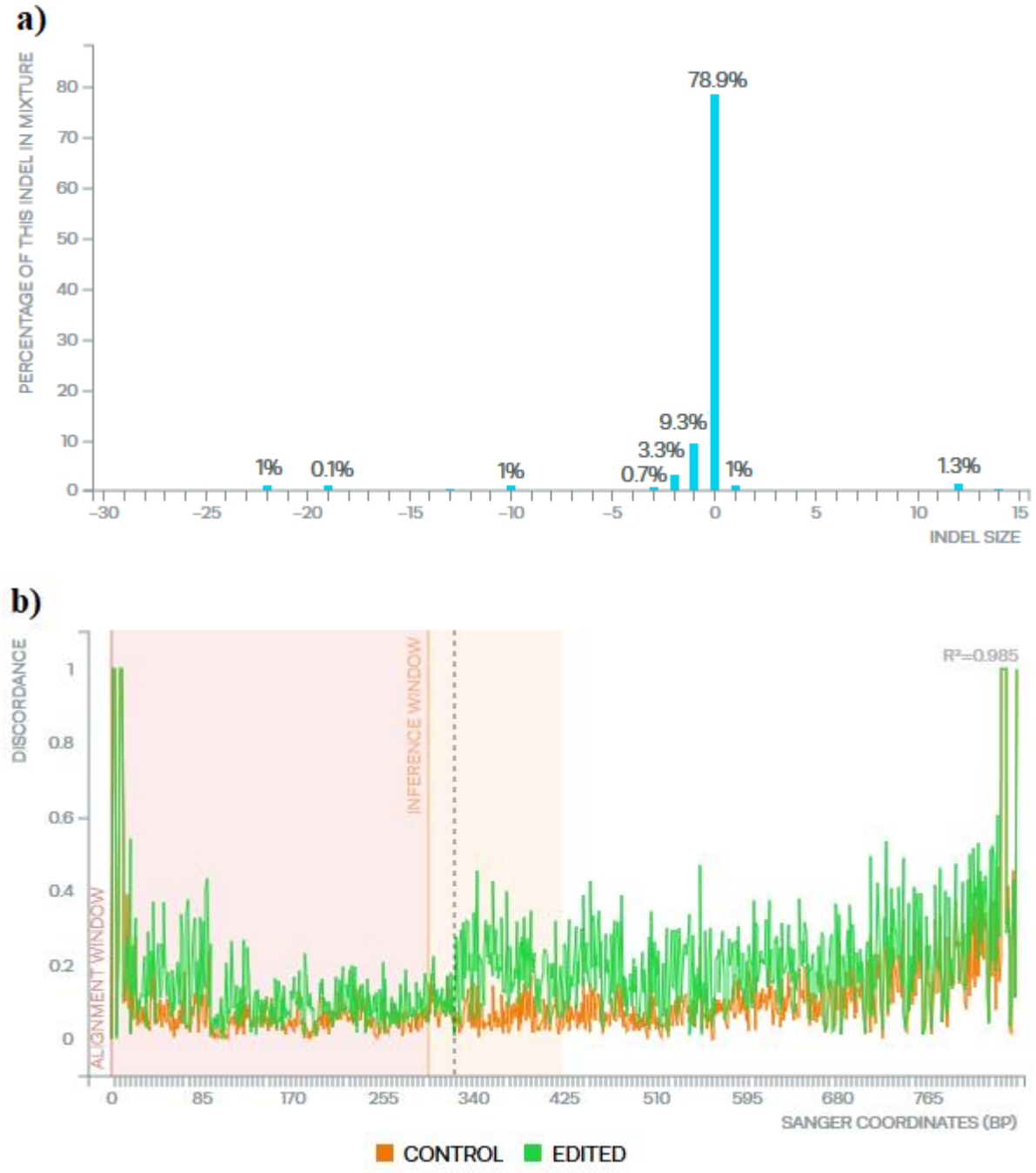

Supplementary Figure 17: Indel distributions with the Indel plot (a). The X-axis on the indel plot represents size of the deletion (on the left side of zero) or insertion (on the right side of zero). Zero represents no indels (or unedited). The Y-axis represents the percentage of the treated sample with a given Indel. The discordance plot (b) shows degree of signal-differences between the treated (edited) and untreated (control) for each base in the sanger-outputs. The alignment window is the region on the sanger output of the control and edited sample that were aligned. The interference window is the located cut-site region. The X-axis is the base pair position on the sequencing output, The Y-axis Is the level of discordance between the edited and control sample. If CRISPR-editing is successful we would expect a high level of discordance at and after the cut-site, but a low level of discordance before the cut-site.

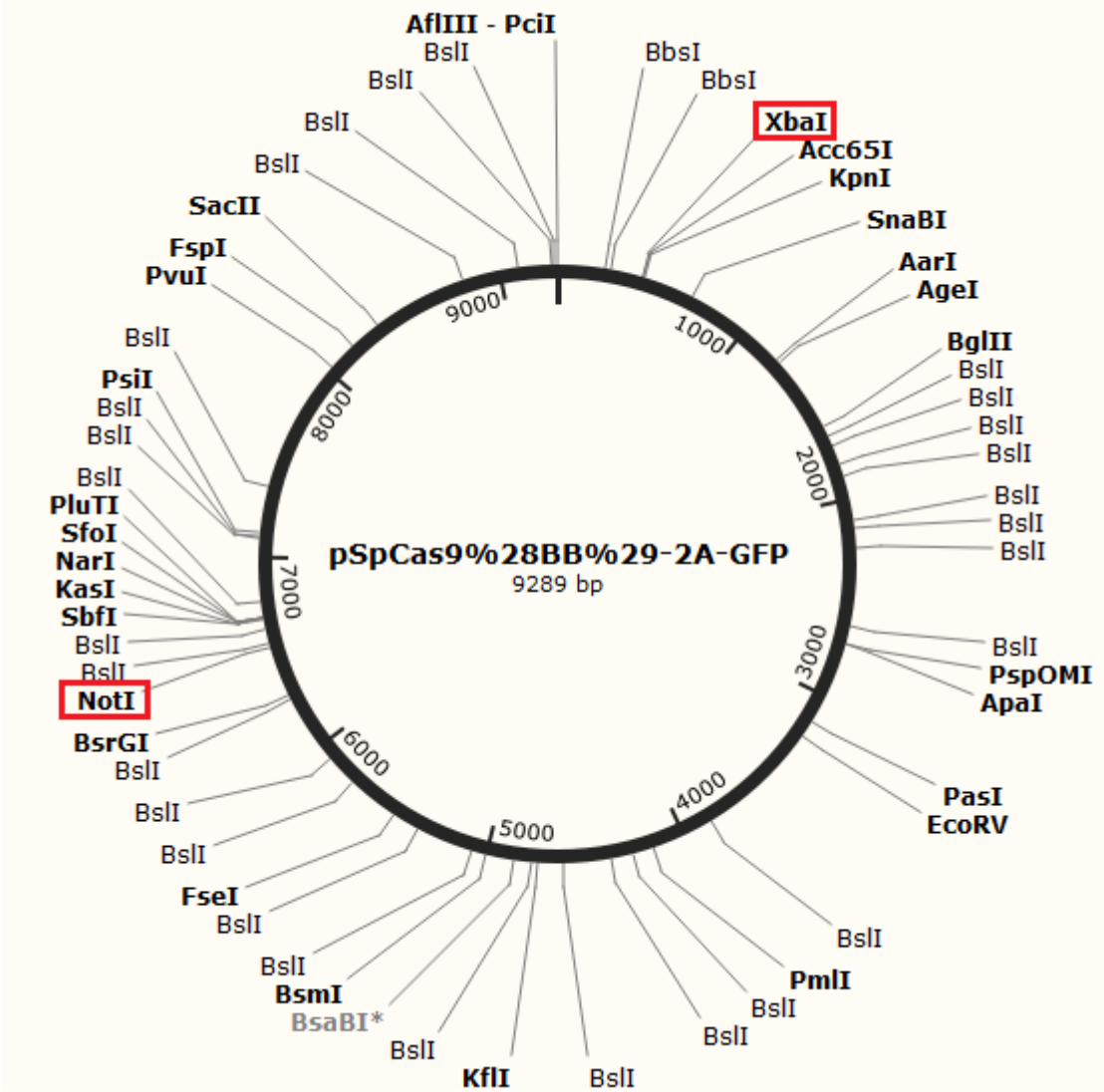

Supplementary Figure 18: The restriction sites of Noti and XbaI, marked with red boxes. Restriction cleavage with both enzymes will generate a smaller 3127 bp fragment, and a larger 6117 bp fragment.